Mon. Not. R. Astron. Soc. **276**, 1155–1178 (1995)

Blue–violet spectral evolution of young Magellanic Cloud clusters

J. F. C. Santos, Jr,[1,★] E. Bica,[1,★] J. J. Clariá,[2,★] A. E. Piatti,[2] L. A. Girardi[1,★] and H. Dottori[1]

[1] *Instituto de Física, Universidade Federal do Rio Grande do Sul, Av. Bento Gonçalves, 9500, Caixa Postal 15051, CEP 91501-970, Porto Alegre, RS, Brazil*

[2] *Observatorio Astronómico, Universidad Nacional de Córdoba, Laprida 854, 5000 Córdoba, Argentina*

Accepted 1995 May 4. Received 1995 April 24; in original form 1994 November 21

ABSTRACT

We study the integrated spectral evolution in the blue–violet range of 97 blue star clusters in the Magellanic Clouds, from those associated with gas emission to those as old as a few hundred Myr. Some clusters are dominated by the flux of those massive stars that pass through evolutionary stages such as Wolf–Rayet, Luminous Blue Variable, Be, and supergiant stars of different temperatures. The relationships among spectral features such as absorption and emission lines, Balmer discontinuity and Balmer continuum are used to study the spectral evolution of the clusters. Finally, we sort into groups spectra of similar evolutionary stages, creating a template spectral library with possible applications in stellar population syntheses of star-forming galaxies and in the spectral simulation of bursts of star formation with different mean ages and durations.

Key words: stars: evolution – Magellanic Clouds – galaxies: star clusters.

1 INTRODUCTION

The Magellanic Cloud clusters are fundamental for understanding the stellar population evolution in galaxies because both the individual stars and the integrated properties can be studied in detail. They span a wide range of ages, allowing one to track the evolution of single burst stellar systems in the metallicity range of the Clouds. The cluster colour–magnitude diagrams (CMDs) provide constraints to stellar evolution models, and the clusters can be used as tracers of the chemical and dynamical evolution of the Magellanic Clouds [see the recent reviews by e.g. van den Bergh (1991) and Westerlund (1990)]. The properties of very young stellar aggregates in the Clouds still undergoing star formation were recently reviewed by Melnick (1992).

The observation of blue populous clusters in the Magellanic Clouds (Hodge 1961) allows one to minimize the effects of the stochastic nature of the integrated properties of star clusters, which otherwise may prove problematic for most young clusters in our Galaxy. Few integrated spectroscopic studies on Magellanic Cloud clusters were made until the early 80's (e.g. Rabin 1982). Integrated spectra of star clusters in the visible and near-infrared ranges were studied by Bica & Alloin (1986, 1987, hereafter BA86, BA87), whose sample contained some Cloud clusters. The near-infrared range for a larger sample of young Cloud clusters was analysed by Bica, Alloin & Santos (1990, hereafter BAS90), in particular the red supergiant phase evidenced by strong TiO bands, as well as Be stars by the presence of Hα emission. An integrated spectral study of Galactic open clusters showed two very young clusters with Wolf–Rayet (WR) features (Santos & Bica 1993). More recently, the near-ultraviolet range of star clusters was explored by Bica, Alloin & Schmitt (1994, hereafter BAS94), part of them belonging to the Clouds, and the behaviour of the Balmer discontinuity and of absorption lines was studied as a function of age and metallicity.

The study of the evolution of young star clusters can contribute to a better understanding of evolutionary phenomena in galaxies. In particular, the evolution of young metal-rich clusters in dense interstellar media might explain the activity in galactic nuclei in terms of evolved massive stars whose effective temperatures are higher than their original zero-age main-sequence value (WARMERs) and supernovae (e.g. Terlevich & Melnick 1985; Cid-Fernandes et al. 1992). The present paper is restricted to studying the cluster evolution at the metallicity values of the Clouds, where interesting phases in the evolution of massive stars occur, such as super-

★ Visiting Astronomer, Complejo Astronómico El Leoncito, which is operated under agreement between the Consejo Nacional de Investigaciones Científicas y Técnicas de la República Argentina and the National Universities of La Plata, Córdoba, and San Juan, Argentina.

giants of different temperatures, and stars with circumstellar gas emission such as Bes, WRs and Luminous Blue Variables (LBVs). Gas emission and dust absorption occur within and around very young clusters, some of which may be embedded in supernova remnants (SNR).

The aim of the present work was to collect a large and deep sample of spectra of young Cloud clusters in order to better understand the integrated light evolution. We chose the blue–violet range because strong spectral changes become apparent as a function of age, and the region is rich in important features such as Balmer and metallic absorption lines, nebular emission lines, stellar emission lines, Balmer discontinuity and Balmer continuum.

In Section 2 the observations and reductions are described and the sample is presented. In Section 3, we provide measurements of continuum points and equivalent widths (W) for absorption and emission features, and discuss the errors. In Section 4 we describe the photometric properties of the sample in terms of its distribution on the integrated $(U-B)\times(B-V)$ diagram. The spectral properties in terms of W and continuum measurements are discussed in Section 5, while in Section 6 the objects presenting similar spectral properties are grouped into templates. Concluding remarks and prospective future work are provided in Section 7.

2 OBSERVATIONS

The observations were carried out with the 2.15-m telescope at the Complejo Astronómico El Leoncito (CASLEO, San Juan, Argentina) in two runs: 1991 October (run A) and 1993 January (run B). We employed the Universidade Federal do Rio Grande do Sul (UFRGS) CCD camera attached to the CASLEO Boller & Chivens spectrograph. The detector is a UV-coated GEC 6803 CCD, with 512×385 pixel each of size 22×22 μm; one pixel corresponds to 1.32 arcsec on the sky. The slit was oriented east–west and the observations were performed by scanning the slit across the object in the north–south direction, in order to get a proper sampling of cluster stars. North–south scans range from 20 to 60 arcsec depending on the object size. In run A we employed a 179 Å mm^{-1} (400 l mm^{-1}) grating and the slit dimensions were 5.5 arcsec × 3.3 arcmin, giving a spectral range of 3600 to 5800 Å, with a mean resolution of 16 Å, according to the FWHM of the He–Ar comparison lamps. In run B we used an 80 Å mm^{-1} (800 l mm^{-1}) grating, a slit of 8.8 arcsec × 3.5 arcmin, resulting a spectral range of 3500 to 4700 Å with a mean resolution of 12 Å. The standard stars observed in run A were HD 205556, BD−15°115 (Gutiérrez-Moreno et al. 1988) and those observed in run B were LTT 3218, LTT 2415, LTT 3864, EG 21 and Hil 600 (Stone & Baldwin 1983).

The reductions were carried out with the IRAF system in a standard way at the Instituto de Física, UFRGS and at the Observatorio Astronómico of the Universidad Nacional de Córdoba. For most objects we have used pixel rows from the same frame for background sky subtraction; a few large objects required background subtraction from a separate frame.

The spectra were calibrated in units of erg s^{-1} cm^{-2} Å^{-1} and they were redshift corrected with $v_r=163$ km s^{-1} and 270 km s^{-1} for the Small Magellanic Cloud (SMC) and the Large Magellanic Cloud (LMC), respectively (Sandage & Tammann 1981). Subsequently, we corrected the spectra for foreground reddening using a normal absorption law (Seaton 1979) and $E(B-V)=0.03$ and 0.06, respectively, for clusters in the SMC and LMC (Mould & Aaronson 1980). Finally, the spectra were normalized to 1 at 4020 Å. These operations were performed with the software SPEED, written by Alex Schmidt for spectral analysis. We have not applied internal reddening corrections, since one of our objectives was to create templates for population synthesis in galaxies, whereby it is suitable to keep the intrinsic reddening in the elements of the data base (Bica 1988).

The sample includes most of the luminous blue star clusters in the Magellanic Clouds as well as H II regions at different stages in their evolution with their embedded stellar content. We list in Table 1 the 83 objects in the LMC followed by the 14 objects in the SMC, all in order of right ascension. By columns: (1) object identifications; (2) observing run; (3) size of aperture extraction in the east–west direction; (4) exposure time; (5) signal-to-noise ratio of the continuum; (6) and (7) integrated UBV colours – for the LMC the data source is from Bica, Clariá & Dottori (1992, hereafter BCD92) and Bica et al. (1995, hereafter BCDSP95), for the SMC the data are from van den Bergh (1981), and some additional sources are indicated in the Table notes; (8) SWB type (Searle, Wilkinson & Bagnuolo 1980, hereafter SWB80), in the case of LMC objects the SWB types are equivalent ones derived from the UBV photometry (BCD92 and BCDSP95), whereas those for the SMC are adopted from SWB80; (9) object nature according to the following convention: C for star cluster, NC for very young cluster embedded in H II region, NA for association embedded in H II region, AN and CN are associations and clusters which show traces of emission, SNR + C is a case of a supernova remnant mixed with a star cluster; (10) ages in Myr for all objects except H II regions, according to BAS90's calibration for foreground-reddening corrected integrated colour $(U-B)_o$; (11) Notes.

3 EQUIVALENT WIDTH MEASUREMENTS

The measurements of equivalent widths (W) and continuum points follow the spectral window definitions for absorption features and the continuum tracings given by BA86 for the range 3988–5314 Å, whereas for the range 3696–3988 Å the definitions are according to BAS94. Equivalent widths are in units of Å. In Table 2 we list by columns: (1) window labels; (2) window limits; (3) main atomic and molecular absorbers in stars; (4) main emission lines in H II regions; (5), (6), (7) and (8) main circumstellar emission lines respectively in Be, LBV, WN and WC stars.

The results of the W measurements are given in Table 3(a) and (b), where negative values indicate emission within the window. The continuum intensities at 3660 and 4570 Å, relative to that at 4020 Å, are listed in Table 4.

The errors on W were estimated from the scatter of the measurements for clusters with multiple observations. The standard star HD 205556, observed in run A once per night (5 spectra with individual $S/N\approx80$ at the continuum level), was used to evaluate night to night statistical fluctuations on the W measurements throughout the run. We derive for the weak ($W<1$ Å) features $\sigma(W)/W<0.4$ and for the strong ($W>7$ Å) ones, $\sigma(W)/W<0.1$. For the cluster NGC 2214

Table 1. The sample.

Name	Run	E-W(")	t(s)	S/N	U-B	B-V	SWB	Class	Age(Myr)	Notes
LMC										
IC2105=N77A (in DEM 4b)	B	23	1200	20	-0.89	-0.10	0	NC	-	
NGC1711=SL55	A	26	780	40	-0.37	0.12	I	C	20	d
NGC1714=N4A=SL64=DEM8b	B	42	600	20	-0.69	-0.10	0	NC	-	
IC2111 (in N79A=BRHT1b,in NGC1722=LH1e,in DEM210)	B	76	1200	20	-0.86	-0.13	0	NC	-	
NGC1731=N4D=LH4=DEM12	B	80	1200	45	-0.84	-0.11	0	NA	< 4	e
KMHK212 (in NGC1731)	B	13	1200	25	-	-	-	C	-	
SL82=KMHK211 (in NGC1731)	B	25	1200	45	-	-	-	CA	-	
NGC1735=SL86	B	34	1200	40	-0.28	0.12	II	C	32	d
NGC1736=N8 (in DEM13)	B	70	1200	20	-0.90	-0.25	0	NA	-	
NGC1743=N83A=SL87 (in DEM22b,in N83=LH5)	B	15	900	10	-0.81	-0.18	0	NC	-	
NGC1755=SL99	B	41	900	45	-0.20	0.16	II	C	55	d
HD32228=KMHK307 (in NGC1761)	A	16	1200	25	-0.91	-0.17	0	C	< 4	e
IC2116=N11A (in N11=DEM34,in N10)	A	11	780	35	-0.80	-0.19	0	NC	-	
HT4 (in NGC1763, in N11)	A	9	780	20	-	-	-	NC	-	
HDE268726=Sk-66°36=HT1 (in N11)	A	11	780	40	-0.76	0.07	-	NC	-	f
NGC1767=SL120 (in LH8=DEM36)	B	21	900	40	-0.58	0.24	I	C	7	d
NGC1772=SL128 (in LH8=DEM36)	A	20	1800	40	-0.56	0.25	I	C	9	
NGC1774=SL141	B	26	1800	40	-0.27	0.20	II	C	37	d
NGC1782=SL140 (in LH8=DEM36)	B	28	1200	40	-0.26	0.25	II	C	36	d
SL153 (sup N10)	B	20	1200	40	-0.15	0.23	III	C	54	
NGC1805=SL186	A	20	780	35	-0.55	0.11	I	C	9	d
NGC1818=SL201	B	38	1200	45	-0.46	0.18	I	C	14	d
NGC1847=SL240	B	45	1200	40	-0.33	0.20	I	C	21	d
Rob1=NGC1850A (in N103B)	A	11	780	45	-0.89	-0.14	0	C	< 4	e
NGC1850=SL261=BRHT5a (in ? N103B)	A	30	780	40	-0.27	0.15	II	C	31	d
NGC1854=NGC1855=SL265	A	106	780	20	-0.27	0.19	II	C	34	d
NGC1872=SL318 (sup N113)	B	32	1800	40	0.06	0.35	IVA	C	136	
NGC1903=SL356 (sup ? DEM130)	B	42	900	45	-0.25	0.14	II	C	44	d
H88-267=SDorCluster (in LH41=DEM132,in N119)	A/B	30	1800	30	-0.69	0.11	I	C	5	
SL360 (in LH41=DEM132,in N119)	A/B	17	1800	50	-0.91	-0.15	0	C	< 4	e
NGC1921w=N121=BRHT49b (in DEM133)	B	14	2100	20	-0.81	0.02	0	NC	-	
NGC1921e=SL381=BRHT49a (in DEM133)	B	19	2100	35	-0.21	0.19	II	C	41	
NGC1935=IC2126=N44B (in SL417,in LH47,in N44)	B	76	1200	20	-0.98	-0.17	0	NC	-	
NGC1936=IC2127=N44C (in SL417,in LH47,in N44)	B	29	1200	20	-0.53	-0.08	0	NC	-	
NGC1949=N138A (in DEM180)	B	68	1200	20	-0.87	-0.22	0	NC	-	
NGC1951=SL464	B	17	900	35	-0.19	0.09	II	C	48	d
NGC1967=SL478 (in DEM198)	A	39	1200	45	-0.75	0.05	I	C	4	
NGC1970 (in SL476=LH58,in N144=DEM199)	B	11	300	40	-0.72	0.15	I	NA	4	
HS314 (in DEM210)	A	24	1200	35	-0.75	-0.11	0	C	4	
NGC1983=LH61 (in DEM210)	A	72	900	40	-0.75	0.16	I	AN	4	
SL492 (in NGC1983=LH61,in DEM210)	A	32	900	45	-0.70	0.16	I	C	5	
NGC1984=SL488 (in DEM210)	A	34	900	40	-0.82	0.01	0	C	< 4	e
NGC1994=SL499 (in DEM210)	A	49	900	50	-0.69	0.09	I	C	6	d
NGC2002=SL517 (in LH77)	A/B	49	1920	40	-0.58	0.34	I	C	8	d
NGC2006=SL537 (in LH77)	A	46	900	40	-0.63	0.12	I	C	5	d
SL538 (in LH77)	A	19	900	40	-0.67	-0.01	0	C	6	d
NGC2009=SL534	A	50	780	25	-0.64	0.27	I	C	6	
NGC2011=SL559=BRHT14a=KMHK1039 (in LH75)	A	22	720	45	-0.71	0.04	I	C	5	d
BRHT14b=KMHK1040 (in LH75)	A	32	900	15	-0.70	0.37	I	C	5	
NGC2021=SL570 (in LH79,in DEM234)	A	40	900	20	-0.77	-0.13	0	C	< 4	e
NGC2025=SL571	B	27	1200	35	-0.07	0.24	III	C	83	d
KMHK1074 (in LH77)	A	18	780	35	-0.80	-0.15	0	C	< 4	e
SL586=ESO86SC12 (in LH77)	A	15	780	40	-0.80	-0.12	0	C	< 4	e
N63A (in NGC2030=SL595, in N63s=LH83)	B	15	1500	15	-0.96	-0.18	0	NC	-	g,h
NGC2032=N59Anw (in LH82,in N59)	B	48	1800	20	-0.58	-0.19	0	NA	-	
BCDSP8 (in NGC2033=SL589=LH81,in N154=DEM246)	A	61	900	35	-0.91	-0.10	0	CN	< 4	a,e
NGC2035=N59A (in LH82,in N59)	B	35	1800	20	-0.76	-0.17	0	NA	-	
NGC2041=SL605	B	40	1200	25	-0.17	0.22	II	C	58	d
SL601=BRHT16a=KMHK1130 (in NGC2042=LH89n)	B	26	1200	30	-0.77	0.18	I	C	< 4	e
BRHT16b=KMHK1131 (in NGC2042=LH89n)	B	25	1800	50	-	-	-	C	-	
LT-α=KMK88-79 (in NGC2044=SL602=LH90,in N157)	A	13	1200	40	-0.52	0.60	I	NC	10	
LT-ζ=KMK88-87 (in NGC2044=SL602=LH90,in N157)	A	15	900	45	-0.65	0.35	I	NC	6	
HDE269828=LT-β=BRHT17b=KMK88-83 (in NGC2044,in N157)	A	52	900	50	-0.82	0.05	0	NC	< 4	e
LT-δ=BRHT17a=KMK88-88 (in NGC2044,in N157)	A	24	900	40	-0.54	0.24	I	CN	10	
LT-γ (in NGC2044, in N157)	A	12	900	50	-	-	-	C	-	
NGC2058=SL614	B	38	1200	25	-0.12	0.24	III	C	62	d

Table 1 – *continued*

Name	Run	E-W(")	t(s)	S/N	U-B	B-V	SWB	Class	Age(Myr)	Notes
LMC										
SL639=M-OB3 (in N157)	A	58	900	25	-0.28	0.60	I	NC	30	
SBCPGD1 (in N157)	A	42	900	15	-	-	-	-	-	b
HS385=M-OB5 (in N160=DEM284,in LH106)	A	18	1000	35	-0.63	0.23	I	C	6	
M-OB4=H88-308	A	24	780	35	-0.53	0.35	I	C	10	
NGC2091=SL653 (in LH106)	A	59	780	25	-0.61	0.38	I	C	7	
NGC2092 (in LH111,in DEM310)	A	54	1200	10	-0.49	0.57	I	C	12	
NGC2096=SL664	A	65	720	25	-0.17	0.49	I	C	49	
NGC2098=SL667	A	36	720	30	-0.58	0.16	I	C	8	d
NGC2100=SL662 (in LH111,in DEM310)	A	45	780	35	-0.56	0.16	I	C	9	d
NGC2102=SL665 (in DEM310)	A	23	1000	35	-0.75	-0.04	0	C	4	
NGC2134=SL760	B	39	1800	30	-0.02	0.26	III	C	124	d
NGC2136=SL762	B	33	1200	35	-0.13	0.28	III	C	58	d
NGC2147=SL784 (in N75B=LH122)	A	26	1500	15	-0.36	0.26	I	CN	21	
NGC2156=SL796	B	28	1200	35	-0.07	0.12	III	C	77	
NGC2159=SL799	B	51	1500	35	-0.14	0.28	III	C	56	
NGC2164=SL808	B	44	1200	40	-0.24	0.10	II	C	44	d
NGC2214=SL860=LW426	B	82	1800	35	-0.27	0.11	II	C	38	d
SMC										
NGC248n=SMC-N13B=SMC-DEM16n=ESO29en8n	B	18	1200	5	-	-	-	NA	-	
NGC248s=SMC-N13A=SMC-DEM16s=ESO29en8s	B	17	1200	10	-	-	-	NC	-	
NGC299=K32=L49=ESO51SC5	A	17	1200	40	-0.44	0.27	I	C	12	d
NGC330=K35=L54=ESO29SC24 (in H-A40)	B	38	1200	45	-0.44	0.17	I	C	13	d
NGC376=K49=L72=ESO29SC29	A	29	1800	35	-0.40	0.27	-	C	20	d
L56	A	17	1200	40	-0.56	0.00	II	C	10	
K50=L74=ESO51SC15 (in H-A54)	A	53	1800	15	-0.60	-0.14	-	C	8	
K54=L79=ESO29SC31 (in B-OB29)	A	30	2700	20	-0.59	0.63	-	C	8	
IC1644=SMC-N81=ESO29en35 (in H-A60)	A	25	1200	25	-	-	-	NC	-	
NGC456=SMC-N83=K65=L94=SMC-DEM147=ESO29SC38=H-A61	B	134	1200	10	-0.98	-	-	NA	-	
SMC-N83A	B	24	1200	20	-	-	-	NC	-	
Sk157 (in NGC465)	B	15	1200	40	-0.94	-0.21	-	C	-	c
Sk158 (in NGC465)	B	12	1200	40	-0.95	-0.18	-	C	-	c
NGC796=L115=WG9=ESO30SC6 (in BS215)	A/B	59	2400	10	-	-0.06	-	C	-	

Notes. Designations in the first column follow BCD92; in parentheses are indicated larger objects where the cluster is located; 'in' suggests coeval objects whereas 'sup' suggests superposition of non-coeval ones; the acronyms LT-, HT, KMHK and BRHT are respectively from Lortet & Testor (1984), Heydari-Malayeri & Testor (1983), Kontizas et al. (1990) and Bhatia et al. (1991).
In column (11): (a) BCDSP8 is a compact cluster in the centre of NGC 2033. (b) SBCPGD1 is a previously anonymous emission region 55 arcsec E and 17 arcsec N of SL639. (c) Photometry values according to Lortet & Testor (1988). (d) Age from the $(U-B)$ and $(u-v)$ calibrations in BAS90. (e) Age extrapolated from the $(U-B)$ calibration in BAS90. (f) *UBV* colours from Heydari-Malayeri & Testor (1983). (g) Colours in a diaphragm of 150 arcsec (more representative of the H II/OB complex NGC 2030 where N63A is embedded). (h) The SNR0535-66.0 occupies the eastern side of N63A.

(run B, three spectra with individual $S/N \approx 30$) we obtained $\sigma(W)/W < 0.2 (W > 4$ Å) and $\sigma(W)/W < 0.3$ ($W \approx 4$–1 Å). For the cluster K54 (run A, three spectra with individual $S/N \approx 15$), we obtained $\sigma(W)/W < 0.2$ ($W > 4$ Å) and $\sigma(W)/W \approx 0.3$–0.8 ($W \approx 4$–1 Å).

For objects presenting nebular and/or circumstellar matter emission, we measured the W of emission lines using a local continuum tracing and present the results in Tables 5(a), (b) and (c) for those with nebular, WR and LBV/Be lines, respectively. Typically $\sigma(W)/W$ is < 0.2 for the emission lines.

4 PHOTOMETRIC PROPERTIES OF THE SAMPLE

The integrated $(U-B)\times(B-V)$ diagram for the LMC sample, using the photometric data from Table 1, is shown in Fig. 1. Although the spatial coverage of the photometric and spectroscopic observations are not identical, Fig. 1 is useful to compare the loci of the various kinds of systems (according to information on the object types in Table 1 and the presence of absorption and emission lines in Tables 3 and 5). The regions of the diagram corresponding to the different SWB types are separated by straight lines. The symbols indicate spectra with different properties: (i) H II region emission lines; (ii) absorption features; (iii) the case of a supernova remnant apparently associated to a cluster (Section 6.3); (iv) the occurrence of LBV/Be emission; (v) WR emission lines and (vi) absorption features plus weak nebular lines. The six objects in the SMC, for which both colours are available (Table 1), have absorption-line spectra.

Since the SWB80 study, dating methods based on comparisons of models using stellar evolutionary tracks with observed CMDs and integrated colours, have shown that the

Table 2. Spectral windows.

Window	Limits(Å)	Stellar Absorption	Nebular Emission	Be Emission	LBV Emission	WN Emission	WC Emission
k	3696-3760	H12,13,..;FeI Mband	[OII];H12,13,..	H12,13,..	H12,13,..	-	-
1L	3780-3810	H10;CN Lband	-	-	-	-	-
2L	3822-3858	H9;CN Lband;FeI;MgI;HeI	-	-	-	-	-
2C	3858-3872		[NeIII]	-	-	-	-
3L	3872-3908	H8;CN Lband;HeI;FeI;SiI	H8	H8;HeI	H8;HeI	-	-
4	3908-3952	CaII K	-	-	-	-	-
5	3952-3988	Hϵ;CaII H	Hϵ;[NeIII]	Hϵ	Hϵ	-	-
6+7	3988-4058	HeI;FeI	HeI	HeI	HeI	NIV	CIII
9	4082-4124	Hδ	Hδ	Hδ	Hδ	-	-
10	4124-4150	FeI	-	-	-	-	-
11	4150-4214	CN	-	-	-	-	-
12	4214-4244	CaI	-	-	[FeII]	-	-
14	4284-4318	CH Gband;FeI;CrI	-	-	[FeII]	-	-
15	4318-4364	Hγ	Hγ;[OIII]	Hγ	Hγ;[FeII]	-	-
18	4450-4484	HeI;TiO;MgII;CaI	HeI	HeI	HeI	-	-
19	4484-4510	CH;CN	-	-	FeII	-	-
21	4568-4622	FeI;TiO;CaI;FeII;TiII;CN	-	-	FeII	NV	CIII-IV
22	4622-4668	FeI;TiO	-	-		NIII	CIII-IV
23	4668-4698	TiO;C_2	-	-	HeII	HeII	CIII-IV
27	4846-4884	Hβ;FeI;TiO	Hβ	Hβ	Hβ	-	-
29	4908-4950	HeI;FeI;FeII;CN	[OIII]	HeI	FeII;HeI	-	-
30	4950-4998	FeI;TiI;TiO	[OIII]	HeI	FeII;HeI	-	-
31	4998-5064	HeI;TiO;CN;FeII;TiI;FeI	[OIII]	HeI	FeII;HeI	-	-
33+34+35	5130-5244	MgI;MgH;FeI;C_2;CrI;TiO;CN	-	-	-	-	-
36	5244-5314	FeI;TiO;CaI;TiI	-	-	-	-	-

Table 3. Equivalent widths in spectral windows.

NAME	k	1L	2L	2C	3L	4	5	6+7	9	10	11	12	14
LMC													
IC 2105	-248.3	-2.9	-6.2	-14.2	-22.2	1.4	-23.8	-2.8	-38.2	-1.0	0.0	-0.1	-0.7
NGC 1711	10.6	4.0	5.7	0.7	6.8	1.4	7.3	1.1	7.0	1.0	0.7	0.7	1.1
NGC 1714	-187.1	-3.6	-9.5	-34.1	-39.6	0.2	-41.6	-6.2	-51.6	-1.2	0.8	0.5	-0.7
IC 2111	-292.1	-3.1	-7.5	-20.2	-25.2	2.0	-27.0	-2.7	-38.3	-0.6	0.2	-0.3	-1.0
NGC 1731	1.2	1.4	1.3	0.3	1.7	1.8	2.8	1.4	1.5	0.5	1.1	0.4	0.3
KMHK 212	7.1	4.2	4.0	0.3	4.8	0.8	5.9	2.4	6.4	2.0	3.0	0.3	1.1
SL 82	0.9	1.2	1.2	0.3	1.3	1.7	2.6	1.2	1.0	0.3	0.8	0.3	0.0
NGC 1735	8.4	3.9	5.3	0.5	6.1	2.2	6.9	1.9	5.7	0.7	0.9	0.3	0.1
NGC 1736	-157.4	-1.6	-5.8	-14.3	-33.2	0.7	-27.2	-2.0	-39.7	-0.8	-0.5	-0.6	-1.1
NGC 1743	-37.1	-0.5	-1.3	-11.6	-13.5	-0.1	-9.0	0.4	-14.7	0.7	0.6	-0.2	-2.0
NGC 1755	12.0	4.9	6.3	0.3	7.4	2.6	8.9	0.9	7.4	0.6	0.9	0.3	1.0
HD 32228	2.4	2.1	2.5	0.3	3.5	1.0	3.1	2.5	3.3	0.7	1.2	0.5	0.6
IC 2116	-148.3	-2.3	-7.4	-28.8	-28.7	-1.3	-31.9	-2.9	-35.4	-0.2	-0.2	0.9	-0.4
HT 4	-280.4	-2.4	-4.6	-8.4	-21.3	-3.3	-17.5	-4.4	-22.3	-1.1	-2.0	1.1	-0.6
HDE 268726	-18.6	1.2	1.7	0.5	0.7	1.8	1.2	1.2	-0.1	0.9	1.5	1.1	-0.2
NGC 1767	8.0	3.6	4.1	0.4	4.8	2.1	6.2	2.4	5.0	0.9	0.7	0.7	0.2
NGC 1772	9.9	4.2	4.1	0.6	6.4	1.8	5.8	2.0	5.7	1.3	0.9	1.3	2.0
NGC 1774	13.4	5.1	6.8	0.2	7.7	3.1	9.0	1.8	7.5	0.6	2.2	0.8	0.9
NGC 1782	10.6	4.7	5.3	0.2	6.4	2.4	7.6	2.0	6.7	1.1	1.2	0.6	1.0
SL 153	12.6	5.4	6.7	0.2	8.0	2.8	10.3	1.1	8.3	0.6	0.8	0.3	0.8
NGC 1805	10.5	3.8	4.9	0.4	5.9	1.0	6.5	2.0	6.6	1.6	1.7	0.9	1.3
NGC 1818	9.2	4.0	4.8	0.2	5.2	1.7	6.9	2.1	5.6	0.7	1.0	0.6	0.3
NGC 1847	9.9	4.6	5.6	0.2	6.1	2.6	8.0	1.7	6.2	0.3	0.8	0.3	0.7
Rob 1	7.4	2.2	3.0	0.5	3.3	0.9	3.3	1.8	3.6	0.6	0.8	0.6	0.4
NGC 1850	11.3	5.1	6.8	0.5	7.3	1.1	7.7	1.1	7.4	0.8	1.0	0.4	1.0
NGC 1854	-0.8	5.4	7.5	0.6	7.4	2.9	8.7	1.5	7.8	1.1	2.2	2.0	2.2
NGC 1872	14.9	6.1	8.4	0.4	9.8	3.0	12.0	1.7	11.3	0.9	1.6	0.7	1.6
NGC 1903	12.3	4.6	6.1	0.4	7.7	3.1	9.4	1.5	7.8	0.7	1.5	0.7	1.3
H88-267	5.0	1.5	-0.3	-0.3	-0.8	-0.2	-1.9	-0.9	-5.3	-0.7	-2.4	-2.0	-3.8
SL 360	4.5	2.0	1.6	0.2	2.6	0.9	3.3	1.0	3.0	0.3	0.3	0.3	0.2
NGC 1921w	-131.3	-0.2	-1.8	-2.7	-7.4	-0.1	-5.1	0.8	-11.4	0.0	1.0	0.2	-0.9
NGC 1921e	4.5	5.0	7.1	0.2	8.3	3.5	9.3	2.3	9.3	1.1	2.4	0.9	1.5
NGC 1935	-151.3	-0.5	-3.2	-5.3	-8.8	-0.9	-8.4	-2.7	-14.7	0.0	0.0	0.2	-0.7
NGC 1936	-174.9	-4.1	-8.7	-65.9	-51.6	2.1	-45.6	-3.0	-39.9	0.4	1.6	1.2	1.6
NGC 1949	-174.4	-3.1	-8.0	-28.9	-28.2	-1.2	-31.0	-2.1	-36.5	0.6	4.0	1.0	0.3

Table 3 – *continued*

NAME	k	1L	2L	2C	3L	4	5	6+7	9	10	11	12	14
LMC													
NGC 1951	8.6	3.3	4.0	0.3	4.7	1.7	6.0	2.6	5.2	0.7	0.9	0.3	0.0
NGC 1967	11.0	2.7	4.2	0.9	4.9	1.0	4.6	1.8	5.1	1.2	0.9	0.7	1.5
NGC 1970	1.7	1.9	2.4	0.4	2.7	2.0	3.0	1.4	2.1	0.9	2.5	1.0	0.2
HS 314	9.2	2.8	3.8	0.5	4.1	1.1	4.0	2.0	4.9	1.4	1.4	0.8	1,5
NGC 1983	6.3	1.6	2.1	0.3	1.2	0.7	2.1	1.9	2.4	0.7	0.8	0.6	1.1
SL 492	6.1	2.0	2.6	0.3	2.9	1.3	3.0	1.7	3.4	0.8	0.8	0.6	1.2
NGC 1984	9.3	2.5	3.3	0.5	3.4	0.9	3.6	1.9	4.2	1.1	1.1	0.8	1.5
NGC 1994	6.8	2.3	2.8	0.4	3.1	0.8	3.0	1.9	3.2	1.2	1.0	0.5	0.6
NGC 2002	3.1	1.2	3.0	0.2	3.7	1.3	4.6	1.6	3.6	0.7	0.9	1.1	1.6
NGC 2006	11.1	3.4	4.4	0.4	5.2	2.2	5.8	1.6	5.7	1.1	1.0	1.1	2.6
SL 538	7.7	2.9	3.4	0.5	3.9	1.2	3.9	1.5	3.9	0.8	0.6	0.5	1.3
NGC 2009	8.9	3.4	3.3	0.9	3.1	0.6	3.6	2.1	5.3	1.4	1.3	0.9	1.9
NGC 2011	5.8	2.3	2.5	0.5	3.4	0.8	2.8	1.2	2.6	0.7	0.2	0.2	0.9
BRHT 14b	4.4	5.0	6.0	0.8	5.4	1.8	6.2	3.4	6.4	1.3	1.6	1.4	2.8
NGC 2021	9.4	3.3	3.5	0.5	6.5	1.4	5.1	3.6	6.2	1.6	1.0	0.4	0.9
NGC 2025	12.4	5.1	6.6	0.5	7.6	2.9	9.4	0.9	7.5	0.5	1.3	0.6	1.3
KMHK 1074	9.0	3.1	3.7	0.7	4.3	1.4	3.8	1.8	4.6	1.2	0.7	0.8	0.7
SL 586	8.5	2.7	3.4	0.6	4.1	0.9	3.8	1.7	4.4	1.0	0.6	0.7	0.5
N 63A	-87.0	-1.0	-3.0	-15.1	-19.4	1.0	-14.8	-0.7	-19.9	-0.8	1.6	1.0	-1.2
NGC 2032	-272.7	-8.4	-17.9	-71.9	-64.6	0.3	-76.2	-7.4	-87.8	-2.1	1.8	0.6	-1.3
BCDSP 8	10.0	2.5	3.5	1.1	4.0	1.5	4.2	1.9	4.7	0.4	0.5	0.7	0.3
NGC 2035	-559.7	-12.6	-26.2	-109.6	-119.7	0.3	-151.7	-14.8	-179.8	-2.9	3.2	-0.5	-1.9
NGC 2041	14.9	4.7	7.4	0.7	7.5	2.5	9.7	2.9	7.9	1.0	3.3	1.4	2.0
SL 601	6.6	2.8	3.4	0.7	4.4	2.3	5.8	2.7	4.6	0.9	1.3	0.4	0.4
BRHT 16b	6.2	2.8	5.8	0.4	5.1	7.9	7.3	2.1	3.3	0.8	3.7	1.3	3.7
LT-α	-8.5	0.5	1.5	0.2	1.0	0.3	0.7	-0.3	0.3	0.3	1.9	0.5	1.4
LT-ζ	3.9	2.3	1.6	0.4	2.4	1.1	3.2	1.7	3.7	0.7	1.0	1.0	1.8
HDE 269828	-1.6	1.9	1.8	0.2	2.4	1.0	2.7	1.5	1.9	0.3	0.8	1.2	1.7
LT-δ	4.5	2.6	2.6	-0.4	4.3	0.8	4.6	2.0	4.7	0.9	1.4	0.8	0.7
LT-γ	5.0	1.7	1.5	0.2	2.5	0.9	1.9	1.6	1.9	0.5	1.6	0.5	0.6
NGC 2058	14.5	6.7	9.8	0.4	8.5	4.6	11.6	3.0	10.0	0.8	4.8	2.4	2.4
SL 639	-11.3	3.3	2.6	0.2	3.3	0.9	3.0	6.1	3.4	2.0	1.7	3.0	2.8
SBCPDG1	-203.2	4.6	-2.3	-8.9	-17.0	1.9	-10.6	3.2	-10.8	3.6	4.5	4.8	-0.7
HS 385	6.9	2.5	3.3	0.5	4.5	1.1	4.8	2.4	5.4	1.3	1.0	1.4	1.1
M-OB4	9.9	3.1	3.6	1.0	3.5	0.4	3.2	1.5	4.5	1.2	1.7	0.8	0.9
NGC 2091	11.5	4.6	5.4	1.1	6.2	1.3	5.6	2.6	6.1	1.3	1.8	2.0	2.4
NGC 2092	3.0	2.9	4.2	-17.0	5.3	-0.2	7.0	6.9	6.3	3.2	7.0	2.7	8.0
NGC 2096	15.4	3.4	5.6	0.3	6.2	9.1	9.1	1.5	4.6	1.2	2.9	2.0	4.2
NGC 2098	10.2	2.7	5.1	0.5	5.4	1.3	4.6	0.8	4.9	1.0	1.1	1.3	1.9
NGC 2100	10.0	3.8	3.7	0.4	3.7	0.5	4.4	1.6	4.9	0.7	1.3	1.4	0.8
NGC 2102	9.8	2.9	4.1	0.7	4.2	1.8	4.7	1.5	5.0	1.0	1.2	1.0	1.2
NGC 2134	17.0	6.9	9.6	0.9	10.9	4.5	13.2	3.3	11.0	1.6	3.2	0.8	1.8
NGC 2136	14.5	5.1	7.4	0.3	7.2	2.7	9.9	1.7	8.2	0.7	2.2	1.2	0.8
NGC 2147	-13.9	5.2	6.3	2.4	6.7	3.1	8.2	6.0	8.4	2.0	4.1	2.5	5.3
NGC 2156	13.0	5.8	6.8	0.3	8.4	3.4	9.9	-0.1	8.0	0.5	1.1	0.9	1.2
NGC 2159	13.3	5.0	7.4	0.3	8.1	3.7	10.2	1.1	8.0	0.6	1.2	0.3	0.6
NGC 2164	10.6	4.8	6.2	0.2	7.6	2.9	9.4	1.7	8.0	0.8	1.0	0.3	0.7
NGC 2214	10.8	4.4	5.9	0.5	6.5	2.5	9.1	1.1	8.6	1.0	1.2	0.4	1.7
SMC													
NGC 248n	-70.6	-1.0	-4.0	-6.0	-13.4	-2.4	-10.7	-4.3	-12.2	0.2	-3.2	0.0	-0.7
NGC 248s	-124.3	-2.2	-4.4	-13.3	-26.6	-0.6	-20.8	-4.7	-23.4	-0.4	0.7	-0.2	-1.6
NGC 299	-	3.4	4.6	0.4	5.1	1.4	6.0	1.9	6.0	1.2	2.0	0.9	1.1
NGC 330	-	3.8	4.5	0.0	4.9	1.5	6.3	1.4	5.5	0.7	1.4	0.6	0.3
NGC 376	-	-	4.8	0.1	4.5	2.7	6.5	1.5	5.1	0.6	2.1	1.5	1.4
L 56	-	4.6	4.9	0.3	6.2	0.8	6.3	1.2	6.4	0.9	1.2	0.2	0.3
K 50	10.3	3.1	4.5	1.1	5.9	1.6	5.9	3.1	7.5	1.6	1.6	1.7	3.4
K 54	7.7	3.2	4.1	0.8	4.7	1.6	4.7	1.3	4.6	1.9	1.9	2.4	3.7
IC 1644	-	-3.4	-5.6	-40.0	-31.5	1.5	-38.4	-2.8	-38.3	-0.8	0.1	-0.2	-1.3
NGC 456	-168.0	0.0	-1.5	-11.4	-20.7	2.2	-17.0	-2.5	-24.4	0.0	1.9	2.6	-0.4
SMC-N83A	-154.4	-1.6	-3.3	-10.1	-20.2	-0.1	-15.3	-1.2	-21.0	-0.6	0.6	0.7	-0.2
Sk 157	4.7	2.2	2.7	0.1	3.1	1.1	4.1	1.0	3.5	0.4	1.3	0.6	0.2
Sk 158	3.4	1.5	2.1	0.3	2.1	1.8	3.0	1.2	2.0	0.4	1.9	0.8	0.4
NGC 796	-	3.8	4.8	1.1	4.8	0.7	6.2	2.7	6.9	1.2	3.1	0.7	0.7

Table 3 – *continued*

NAME	15	18	19	21	22	23	27	29	30	31	33+34+35	36
LMC												
IC 2105	-84.2	-8.4	-0.5	2.3	1.3	1.0	-	-	-	-	-	-
NGC 1711	6.8	0.9	0.1	0.6	0.5	0.8	5.5	0.5	0.7	1.8	2.6	1.7
NGC 1714	-111.5	-11.7	-0.9	4.0	-0.2	0.5	-	-	-	-	-	-
IC 2111	-89.6	-8.9	-1.0	3.2	3.0	1.5	-	-	-	-	-	-
NGC 1731	1.9	0.9	0.1	1.8	0.7	0.4	-	-	-	-	-	-
KMHK 212	4.7	3.1	1.2	4.2	3.0	0.5	-	-	-	-	-	-
SL 82	1.5	0.6	-0.2	1.1	0.2	0.2	-	-	-	-	-	-
NGC 1735	5.0	0.6	-0.1	1.8	0.7	0.4	-	-	-	-	-	-
NGC 1736	-90.1	-10.0	-1.0	3.3	2.4	1.5	-	-	-	-	-	-
NGC 1743	-35.1	-4.1	-2.0	6.1	1.3	1.2	-	-	-	-	-	-
NGC 1755	7.4	0.4	-0.1	1.2	0.6	0.5	-	-	-	-	-	-
HD 32228	3.3	1.5	0.2	-7.2	-30.3	-13.0	2.2	1.0	1.0	1.2	2.2	0.8
IC 2116	-84.8	-8.7	-0.6	-1.0	-3.3	1.1	-253.8	-15.3	-397.8	-1196.3	-3.0	-1.2
HT 4	-53.9	-6.3	-1.2	-4.6	-4.1	0.9	-151.2	-6.7	-135.0	-415.4	1.9	4.0
HDE 268726	-2.1	0.2	-0.3	0.5	0.9	0.2	-9.5	-0.3	-3.0	-6.8	0.7	-0.1
NGC 1767	5.0	0.8	0.0	0.9	0.9	0.3	-	-	-	-	-	-
NGC 1772	7.5	2.3	0.7	0.8	1.0	0.6	3.9	0.5	0.8	2.2	4.1	2.3
NGC 1774	7.2	0.5	-0.1	1.5	0.5	0.4	-	-	-	-	-	-
NGC 1782	7.0	1.0	0.0	0.8	0.7	0.7	-	-	-	-	-	-
SL 153	8.0	0.4	0.3	0.9	0.8	0.4	-	-	-	-	-	-
NGC 1805	6.0	1.8	0.3	1.3	1.4	0.8	4.7	0.4	1.8	4.1	6.7	4.5
NGC 1818	5.3	1.0	0.1	1.2	1.0	0.3	-	-	-	-	-	-
NGC 1847	6.7	0.7	0.2	1.6	1.1	0.6	-	-	-	-	-	-
Rob 1	3.3	1.1	0.3	0.5	0.3	1.0	2.9	0.4	0.2	1.4	1.7	1.3
NGC 1850	7.1	0.8	0.0	0.6	0.7	0.7	6.8	0.4	0.3	1.8	3.2	2.1
NGC 1854	7.3	1.8	0.7	0.6	0.1	1.6	3.2	-0.7	-2.8	-11.4	3.5	1.1
NGC 1872	11.4	0.2	0.0	1.3	0.6	0.4	-	-	-	-	-	-
NGC 1903	7.9	0.9	0.3	1.4	1.0	0.4	-	-	-	-	-	-
H88-267	-13.6	-2.2	-3.0	-4.0	-2.4	-0.3	28.5	-2.8	-0.7	-3.9	-8.3	-5.6
SL 360	3.3	0.8	-0.2	-1.2	-2.7	-1.9	2.0	1.0	0.9	2.0	1.2	0.3
NGC 1921w	-31.3	-3.9	-0.7	0.1	-0.6	-0.2	-	-	-	-	-	-
NGC 1921e	8.3	0.6	0.3	2.6	1.0	1.2	-	-	-	-	-	-
NGC 1935	-35.4	-3.0	-0.2	2.3	2.5	0.6	-	-	-	-	-	-
NGC 1936	-83.4	-7.0	-1.1	2.0	0.0	-10.7	-	-	-	-	-	-
NGC 1949	-82.5	-7.1	0.3	3.2	2.9	2.2	-	-	-	-	-	-
NGC 1951	4.9	0.5	-0.3	1.8	0.9	0.3	-	-	-	-	-	-
NGC 1967	6.3	1.9	0.3	1.1	0.6	0.9	3.5	0.3	0.7	2.7	2.8	1.9
NGC 1970	1.0	1.8	0.3	4.4	3.0	0.5	-	-	-	-	-	-
HS 314	6.0	1.6	0.0	1.1	1.0	0.6	2.3	1.0	0.6	1.4	1.7	0.9
NGC 1983	2.6	0.9	0.3	0.7	0.2	0.1	-1.0	0.5	0.3	0.3	3.1	2.0
SL 492	4.1	1.4	0.2	0.4	0.6	0.5	2.1	0.8	0.8	2.7	4.6	3.0
NGC 1984	5.3	1.7	0.3	0.7	1.2	0.7	2.2	0.5	1.2	1.9	2.5	1.7
NGC 1994	2.3	1.5	0.3	0.9	0.6	1.0	-5.4	0.0	1.1	1.1	1.8	1.5
NGC 2002	4.6	1.0	-0.3	0.5	0.8	0.3	2.3	0.5	2.2	4.2	10.8	6.2
NGC 2006	7.0	1.4	0.3	1.0	0.5	0.6	3.7	0.3	0.1	1.4	2.0	1.6
SL 538	5.0	1.5	0.3	0.6	0.5	0.7	2.7	0.7	0.8	2.2	3.1	2.2
NGC 2009	4.4	2.5	0.6	1.3	1.0	0.3	3.1	-0.1	0.9	2.6	5.4	4.1
NGC 2011	3.9	1.4	0.4	0.4	0.7	0.7	2.0	0.3	1.0	2.3	2.1	2.2
BRHT 14b	6.2	3.0	0.1	2.2	3.9	1.9	6.0	3.8	5.0	9.2	13.2	9.4
NGC 2021	3.8	3.0	1.0	1.8	-0.8	1.8	1.4	2.4	0.0	-1.1	4.3	4.0
NGC 2025	7.6	1.1	0.3	1.7	0.9	0.7	-	-	-	-	-	-
KMHK 1074	5.1	1.8	0.6	0.6	1.0	0.8	2.6	0.8	1.0	1.6	3.7	2.2
SL 586	4.1	1.4	0.4	0.7	0.5	0.9	2.8	0.5	0.3	1.9	2.0	1.7
N 63A	-52.6	-5.5	-1.2	2.5	0.1	1.0	-	-	-	-	-	-
NGC 2032	-180.6	-17.8	-1.9	3.9	1.2	0.7	-	-	-	-	-	-
BCDSP 8	3.8	1.6	0.6	0.8	1.4	0.1	3.6	1.0	0.7	0.7	2.1	1.3
NGC 2035	-373.9	-22.2	3.9	11.2	4.4	1.7	-	-	-	-	-	-
NGC 2041	8.5	2.4	0.5	3.3	1.5	0.4	-	-	-	-	-	-
SL 601	3.7	1.5	0.0	1.0	0.7	0.4	-	-	-	-	-	-
BRHT 16b	4.3	1.0	0.6	3.4	2.2	0.6	-	-	-	-	-	-
LT-α	0.8	0.5	-0.5	-3.0	-8.1	-8.0	-4.2	-0.1	-4.0	-13.0	2.8	1.9
LT-ζ	4.4	1.8	0.5	0.9	0.9	1.0	0.2	0.4	-0.8	-3.1	0.9	1.3
HDE 269828	3.3	1.4	0.3	0.1	-1.2	-6.1	-2.3	0.2	-2.6	-6.7	0.6	0.8
LT-δ	4.2	1.5	0.0	0.2	0.8	0.4	1.5	-0.7	-2.8	-6.0	1.3	1.4
LT-γ	2.7	0.9	0.3	1.3	0.1	0.1	-0.3	-1.0	-2.3	-5.0	-0.3	0.3
NGC 2058	9.4	1.3	0.7	3.2	2.9	1.2	-	-	-	-	-	-
SL 639	1.8	3.0	1.4	1.9	1.5	1.1	-6.2	-1.6	-9.3	-24.5	1.2	1.6
SBCPGD1	-34.2	-0.2	1.4	2.7	-0.3	-1.0	-93.2	-2.4	-111.0	-324.9	4.2	1.1
HS 385	4.8	1.5	0.2	1.4	1.7	1.1	3.8	0.9	1.4	2.3	3.5	2.7

Table 3 – *continued*

NAME	15	18	19	21	22	23	27	29	30	31	33+34+35	36
LMC												
M-OB4	4.2	1.5	0.5	0.7	0.9	1.1	3.2	0.7	1.3	2.1	4.7	2.5
NGC 2091	6.2	2.3	0.8	2.7	1.0	1.2	4.4	1.1	3.1	6.1	8.2	5.7
NGC 2092	8.7	4.3	3.9	5.9	5.1	0.4	0.8	0.0	2.1	8.9	1.5	2.5
NGC 2096	6.8	2.6	0.6	1.1	0.4	0.2	5.1	1.9	1.6	2.9	7.0	4.3
NGC 2098	6.6	1.2	0.2	0.7	1.2	0.1	3.1	0.6	1.0	2.4	4.2	2.8
NGC 2100	4.3	1.3	0.0	0.7	0.5	0.8	3.9	1.0	1.1	3.0	3.8	2.2
NGC 2102	4.7	1.3	0.4	0.9	1.0	0.5	3.4	0.8	0.6	1.9	1.9	1.7
NGC 2134	9.8	0.8	0.3	1.5	0.8	0.4	-	-	-	-	-	-
NGC 2136	7.4	0.7	-0.1	1.1	1.5	0.7	-	-	-	-	-	-
NGC 2147	6.9	3.1	1.9	2.8	0.3	0.6	1.0	3.2	1.5	2.5	9.3	5.6
NGC 2156	9.0	0.9	0.5	1.7	0.8	0.7	-	-	-	-	-	-
NGC 2159	7.9	0.8	-0.2	1.1	0.8	1.3	-	-	-	-	-	-
NGC 2164	7.6	0.0	-0.2	1.0	0.4	0.3	-	-	-	-	-	-
NGC 2214	8.1	0.9	0.5	1.8	0.7	0.6	-	-	-	-	-	-
SMC												
NGC 248n	-28.2	-2.7	-1.1	3.2	1.2	2.0	-	-	-	-	-	-
NGC 248s	-55.7	-4.4	-1.0	2.7	2.2	1.6	-	-	-	-	-	-
NGC 299	4.1	1.8	0.0	0.6	1.0	0.2	3.9	1.4	0.0	2.2	5.3	2.9
NGC 330	5.0	0.4	-0.1	1.1	0.5	0.3	-	-	-	-	-	-
NGC 376	5.9	2.2	0.6	1.6	1.3	1.0	4.4	1.5	0.3	2.7	4.4	2.1
L 56	6.0	1.1	0.2	0.4	0.6	0.5	4.6	1.2	0.5	1.4	2.7	0.6
K 50	8.6	3.5	1.3	0.8	2.5	0.8	3.9	1.5	1.1	3.8	3.2	1.0
K 54	6.8	3.2	0.5	1.4	0.5	1.1	2.6	0.8	2.0	3.8	9.2	4.9
IC 1644	-97.1	-8.3	-0.7	-1.0	-1.3	1.0	-262.2	-2.0	-495.9	-1561.9	6.7	2.2
NGC 456	-55.3	-4.2	0.0	1.9	2.0	-0.6	-	-	-	-	-	-
SMC-N83A	-47.9	-4.1	-0.1	2.1	2.2	0.6	-	-	-	-	-	-
Sk 157	3.9	0.9	0.0	0.7	0.4	0.6	-	-	-	-	-	-
Sk 158	2.6	0.4	-0.2	1.0	0.8	0.4	-	-	-	-	-	-
NGC 796	5.4	1.7	1.3	1.6	1.8	2.8	6.0	3.1	0.4	3.6	6.8	6.5

Table 4. Continuum points.

Name	$\frac{F(3640)}{F(4020)}$	$\frac{F(3660)}{F(4020)}$	$\frac{F(4570)}{F(4020)}$	Name	$\frac{F(3640)}{F(4020)}$	$\frac{F(3660)}{F(4020)}$	$\frac{F(4570)}{F(4020)}$	Name	$\frac{F(3640)}{F(4020)}$	$\frac{F(3660)}{F(4020)}$	$\frac{F(4570)}{F(4020)}$
LMC				*LMC*				*LMC*			
IC 2105	1.8	1.5	0.7	NGC 1949	2.3	1.8	0.8	HS 385	-	0.6	0.8
NGC 1711	-	0.5	0.7	NGC 1951	-	0.9	0.7	M-OB4	-	0.7	0.8
NGC 1714	2.1	1.7	1.0	NGC 1967	-	0.7	0.7	NGC 2091	-	0.6	0.9
IC 2111	1.9	1.6	0.8	NGC 1970	-	1.0	0.7	NGC 2092	-	0.6	0.9
NGC 1731	-	1.1	0.7	HS 314	-	0.7	0.7	NGC 2096	-	0.5	1.0
KMHK 212	-	1.0	0.6	NGC 1983	-	0.7	0.7	NGC 2098	-	0.6	0.7
SL 82	-	1.2	0.7	SL 492	-	0.6	0.7	NGC 2100	-	0.6	0.7
NGC 1735	-	0.6	0.7	NGC 1984	-	0.7	0.7	NGC 2102	-	0.7	0.7
NGC 1736	2.0	1.7	0.7	NGC 1994	-	0.7	0.7	NGC 2134	-	0.4	0.8
NGC 1743	1.5	1.3	0.6	NGC 2002	-	0.9	0.8	NGC 2136	-	0.5	0.8
NGC 1755	-	0.6	0.8	NGC 2006	-	0.6	0.8	NGC 2147	-	0.5	0.8
HD 32228	-	-	0.7	SL 538	-	0.6	0.7	NGC 2156	-	0.5	0.8
IC 2116	-	1.0	0.7	NGC 2009	-	0.6	0.8	NGC 2159	-	0.6	0.8
HT 4	-	0.7	0.6	NGC 2011	-	0.6	0.7	NGC 2164	-	0.6	0.8
HDE 268726	-	0.8	0.7	BRHT 14b	-	0.5	0.5	NGC 2214	-	0.6	0.8
NGC 1767	-	0.9	0.8	NGC 2021	-	0.8	0.7				
NGC 1772	-	0.6	0.7	NGC 2025	-	0.6	0.8	*SMC*			
NGC 1774	-	0.5	0.7	KMHK 1074	-	0.7	0.7				
NGC 1782	-	0.7	0.8	SL 586	-	0.7	0.7	NGC 248n	1.5	1.4	0.8
SL 153	-	0.6	0.8	N 63A	-	1.5	0.7	NGC 248s	1.6	1.3	0.7
NGC 1805	-	0.6	0.7	NGC 2032	2.8	2.2	0.8	NGC 299	-	-	0.8
NGC 1818	-	0.8	0.8	BCDSP 8	-	0.7	0.7	NGC 330	-	-	0.7
NGC 1847	-	0.6	0.8	NGC 2035	4.8	3.5	0.7	NGC 376	-	-	0.8
Rob 1	-	0.8	0.6	NGC 2041	-	0.5	0.8	L 56	-	-	0.7
NGC 1850	-	0.4	0.8	SL 601	-	1.1	0.8	K 50	-	0.7	0.7
NGC 1854	-	0.4	0.7	BRHT 16b	-	0.4	1.0	K 54	-	0.7	0.9
NGC 1872	-	0.4	0.9	LT-α	-	0.6	1.0	IC 1644	-	-	0.7
NGC 1903	-	0.6	0.8	LT-ζ	-	0.7	0.8	NGC 456	1.5	1.4	0.7
H88-267	-	0.9	0.7	HDE 269828	-	0.6	0.7	SMC-N83A	1.6	1.4	0.7
SL 360	-	1.2	0.7	LT-δ	-	0.5	0.8	Sk 157	-	1.1	0.6
NGC 1921w	1.3	1.2	0.7	LT-γ	-	0.8	0.7	Sk 158	-	1.2	0.7
NGC 1921e	-	0.6	0.8	NGC 2058	-	0.5	0.9	NGC 796	-	-	0.4
NGC 1935	1.5	1.4	0.7	SL 639	-	0.6	0.9				
NGC 1936	1.8	1.5	0.9	SBCPGD1	-	1.1	1.5				

Table 5. (a) Equivalent widths of emission lines: nebular.

NAME	[OII] 3727	[NeIII] 3868	Hε+[NeIII] 3968	Hδ 4100	Hγ 4340	[OIII] 4363	HeI 4471	Hβ 4861	[OIII] 4959	[OIII] 5007
LMC H II regions										
IC 2105	-242.6	-16.1	-23.8	-38.2	-92.5	-5.3	-8.4	-	-	-
NGC 1714	-170.6	-45.8	-41.6	-51.6	-101.4	-4.5	-11.7	-	-	-
IC 2111	-254.7	-24.5	-27.0	-38.3	-83.1	-2.8	-8.9	-	-	-
NGC 1736	-143.5	-24.7	-27.2	-39.7	-86.1	-3.9	-10.0	-	-	-
NGC 1743	-42.9	-13.6	-9.0	-14.7	-32.0	-	-4.1	-	-	-
IC 2116	-153.9	-32.3	-31.9	-35.4	-113.1	-11.7	-8.7	-253.8	-334.9	-1038.9
HT 4	-362.3	-11.7	-17.5	-22.3	-49.9	-1.9	-6.3	-151.2	-126.6	-393.6
NGC 1921w	-140.7	-3.5	-5.1	-11.4	-30.2	-	3.9	-	-	-
NGC 1935	-155.2	-6.1	-8.4	-14.7	-38.6	-1.6	-3.0	-	-	-
NGC 1936	-142.0	-87.9	-45.6	-39.9	-79.6	-13.0	-7.0	-	-	-
NGC 1949	-153.9	-32.2	-31.0	-36.5	-92.8	-4.8	-7.1	-	-	-
NGC 2032	-228.1	-90.1	-76.2	-87.8	-148.9	-6.8	-17.8	-	-	-
NGC 2035	-458.2	-121.9	-151.7	-179.8	-377.2	-24.0	-22.2	-	-	-
BSCPGD1	-205.2	-17.5	-10.6	-10.8	-32.2	-5.4	-0.2	-93.2	-104.9	-335.3
SMC H II regions										
NGC 248n	-68.7	-10.3	-10.6	-12.2	-25.7	-3.0	2.7	-	-	-
NGC 248s	-120.8	-23.3	-20.8	-23.4	-49.8	-4.5	-4.4	-	-	-
IC 1644	-	-50.6	-38.4	-38.3	-80.1	-12.3	-8.3	-262.2	-429.7	-1328.1
NGC 456	-173.8	-16.3	-17.0	-24.4	-52.7	-5.3	-4.2	-	-	-
SMC-N83A	-138.1	-14.8	-15.3	-21.0	-45.5	-2.7	-4.1	-	-	-
LMC HII region+cluster+SNR										
N 63A	-84.4	-24.6	-14.8	-19.8	-47.4	-7.9	-5.5	-	-	-
LMC Objects with weak nebular lines										
HDE 268726	-23.6	-	-1.2	-0.1	-1.7	-	-0.2	-9.5	-2.2	-6.6
NGC 1854	-14.9	-	-8.7	-7.8	-7.3	-	-1.8	-3.2	-3.6	-12.8
BCDSP 8	-	-	-4.2	-4.7	-3.8	-	-1.6	-3.6	-0.7	-1.1
LT-ζ	-4.4	-	-3.2	-3.7	-4.4	-	-1.8	-0.2	-1.2	-3.6
LT-δ	-6.0	-0.4	-4.6	-4.7	-4.2	-	-1.5	-	-2.4	-6.1
LT-γ	-	-	-1.9	-1.9	-2.7	-	-0.9	-0.3	-2.2	-4.8
SL 639	-23.5	-	-3.0	-3.4	-1.8	-	-3.0	-6.2	-8.3	-24.8
NGC 2092	-	-20.1	-7.0	-6.3	-8.7	-	-4.3	-0.8	-3.0	-9.8
NGC 2147	-34.9	-	-8.2	-8.4	-6.9	-	-3.1	-1.0	-	-

Table 5. (b) Equivalent widths of emission lines: WR.

NAME	[OII] 3727	NIV 4058	NV 4603/19	NIII 4640	CIII/IV 4650	HeII 4686	Hβ 4861	[OIII] 4959	[OIII] 5007
LMC WR									
HD 32228	-	-	-	-	-52.0	-	-	-	-
SL 360	-	-	-	-	-6.7	-	-	-	-
NGC 2021	-6.4	-	-	-0.8	-	-	-	-1.8	-4.7
LT-α	-10.8	-1.1	-3.0	-8.1	-	-8.0	-4.2	-5.2	-15.1
HDE 269828	-4.7	-	-	-1.2	-	-6.1	-2.3	-2.6	-8.2

Table 5. (c) Equivalent widths of emission lines: LBV, Be.

NAME	Hε+[NeIII] 3968	Hδ 4100	Hγ 4340	HeI 4471	FeII 4515	FeII 4584	Hβ 4861	FeII+HeI 4923	FeII+HeI 5018
LMC LBV									
H88-267	-0.9	-5.3	-13.6	-2.2	-3.5	-2.7	-28.5	-2.8	-3.9
LMC Be									
NGC 1983	-	-	-	-	-	-	-1.0	-	-
NGC 1994	-	-	-	-	-	-	-5.4	-	-

sequence of the blue clusters in the colour–colour diagram is basically an evolutionary path (see Girardi & Bica 1993, hereafter GB93, for a recent discussion based on the *UBV* photometry for the 624 LMC clusters in BCD92 and BCDSP94). In the subsequent discussions the CMD groups of Galactic open clusters, together with their turnoff spectral types and ages by Mermilliod (1981a, b), were useful guidelines for inferences on the stellar content of young clusters. The SWB0 region in Fig. 1 contains H II regions (with their embedded stellar content), as well as some very blue star

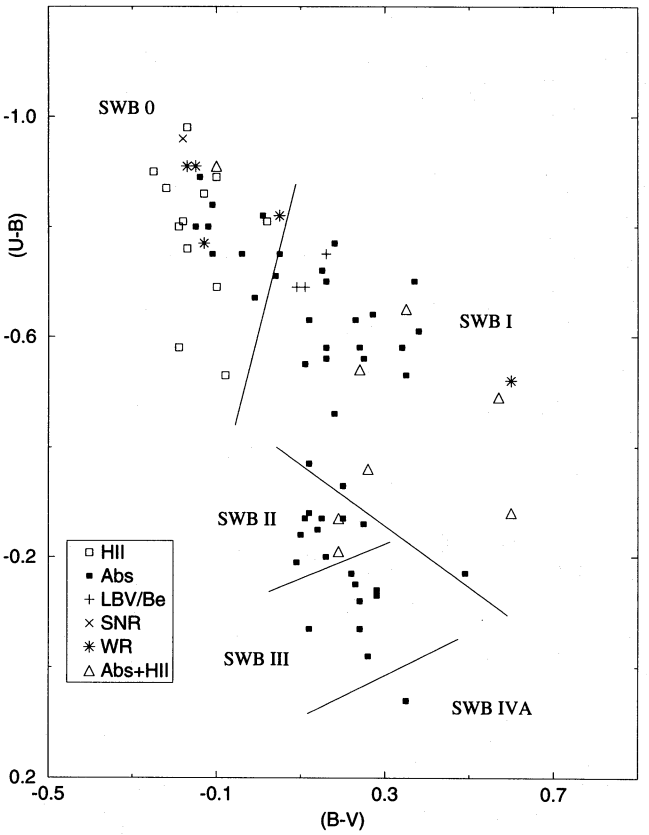

Figure 1. Distribution of LMC objects in the integrated *UBV* colour–colour diagram. Straight lines separate the SWB type regions. Age increases from SWB 0 to IVA. Symbols distinguish the most evident spectral characteristics.

clusters which are free of nebular lines owing to the evolution of ionizing stars and/or gas sweeping by stellar winds (see Section 6.2). After the H II region phase, the most populated regions of the diagram in Fig. 1 are dominated by absorption-line clusters, which define the evolutionary path throughout SWB I, II and III to SWB IVA (ages varying from ≈ 6 to ≈ 150 Myr). In the SWB I phase some clusters reach redder integrated colours by the occurrence of red supergiant stars (BAS90, GB93) whereas clusters in the SWB II type become bluer. Blue supergiants can occur around the SWB 0/SWB I borderline, as suggested by simple spectral syntheses (see Section 6.1). The three cases of LBV/Be emission are in the SWB I region, close to the SWB 0 boundary. Although LBV and Be belong to different stellar evolutionary stages, their corresponding cluster integrated colours in the present sample occupy similar loci in the diagram. The objects with WR stars occur in the SWB 0 region, except the cluster LT-α which contains, in addition, a red supergiant flux contribution (Section 6.2). The objects with absorption plus weak nebular lines (Abs + H II) are distributed in the SWB 0, I and II regions (Fig. 1) and include cases from the latest H II region evolutionary stages to clusters belonging to older parts of currently star-forming complexes, as well as considerably older clusters which may be projected or even embedded in environmental gas of currently star-forming complexes (Section 6.4).

The sample is large enough to map the evolutionary path of young systems in the LMC on the $(U-B)\times(B-V)$ plane. Cases of deviating objects on the plane can be analysed in detail by means of their integrated spectra. Consequently, the young stellar population component of the LMC is studied both quantitatively, by the inclusion in the sample of most of the luminous blue clusters, and qualitatively, since the spectra show features denoting the presence of most products of the evolution of massive stars.

5 SPECTRAL PROPERTIES OF THE SAMPLE

The spectral properties of the objects in the H II region phase are analysed in Fig. 2 for two emission lines from Table 5(a). W(He I–4471 Å) correlates with $W(\mathrm{H}\gamma)$ (Fig. 2a) and with the Balmer discontinuity, as measured by the flux ratio F(3640 Å)/F(4020 Å) (Fig. 2b). The larger W(He I–4471 Å) and $W(\mathrm{H}\gamma)$, the higher the gas excitation and the younger the object, since $W(\mathrm{H}\gamma)$ will basically follow the behaviour of $W(\mathrm{H}\beta)$, which decreases with age owing mostly to the smaller number of Lyman continuum photons caused by the evolution of ionizing stars (Copetti, Pastoriza & Dottori 1986, hereafter CPD86, and references therein). The Balmer discontinuity in emission observed in very excited H II regions is mainly a consequence of two factors: (i) the essentially absent Balmer absorption discontinuity in the stellar component, which is dominated by O and early B stars (see e.g. the stellar spectra in the library of Jacoby, Hunter & Christian 1984, hereafter JHC84); and (ii) the H I Balmer continuum emission in the gas produced by free–bound recombinations. Fig. 2(c) shows that W(He I–4471 Å) is also correlated to $(U-B)$, although the spread is larger than those in Figs 2(a) and (b), possibly owing to the different sizes of photometric and spectroscopic observations; this correlation is in the sense that more excited H II regions are *redder* in $(U-B)$ than less excited ones (see Section 6.5).

The basic properties of the objects dominated by absorption lines can be deduced from Fig. 3, for a selection of features from Table 3. We show the equivalent width of a metallic feature [W(K Ca II)] as a function of $(U-B)$ in Fig. 3(a); W decreases for bluer clusters, which is *not* a metallicity effect: it is caused by age, as a consequence of hotter and brighter turnoffs in younger clusters, which contribute to the continuum flux and not to the metallic line, diluting its absorption (BA86). We show W(K Ca II) against a Balmer line [$W(H\delta)$] in Fig. 3(b). The behaviour is similar to that in Fig. 3(a) because Balmer absorption lines are a good age indicator for blue clusters and have their maximum strength in clusters with turnoff in A0 stars (BA86; Mermilliod 1981a), i.e. around 250 Myr. Two clusters deviate from the relation in Fig. 3(b) (in Fig. 3a one of them has no *UBV* data); they have strong K Ca II lines, which corresponds to cases of F supergiant components dominating the integrated light (see Section 6.1). In Fig. 3(c) we compare Ws of two Balmer lines, which define a ranking of the clusters in age, the older ones having the largest values of $W(\mathrm{H}\delta)$ and $W(\mathrm{H}\gamma)$.

6 SPECTRAL GROUPS

In the present work we are dealing with three basic types of spectra: (i) those in which gas emission dominates over stellar

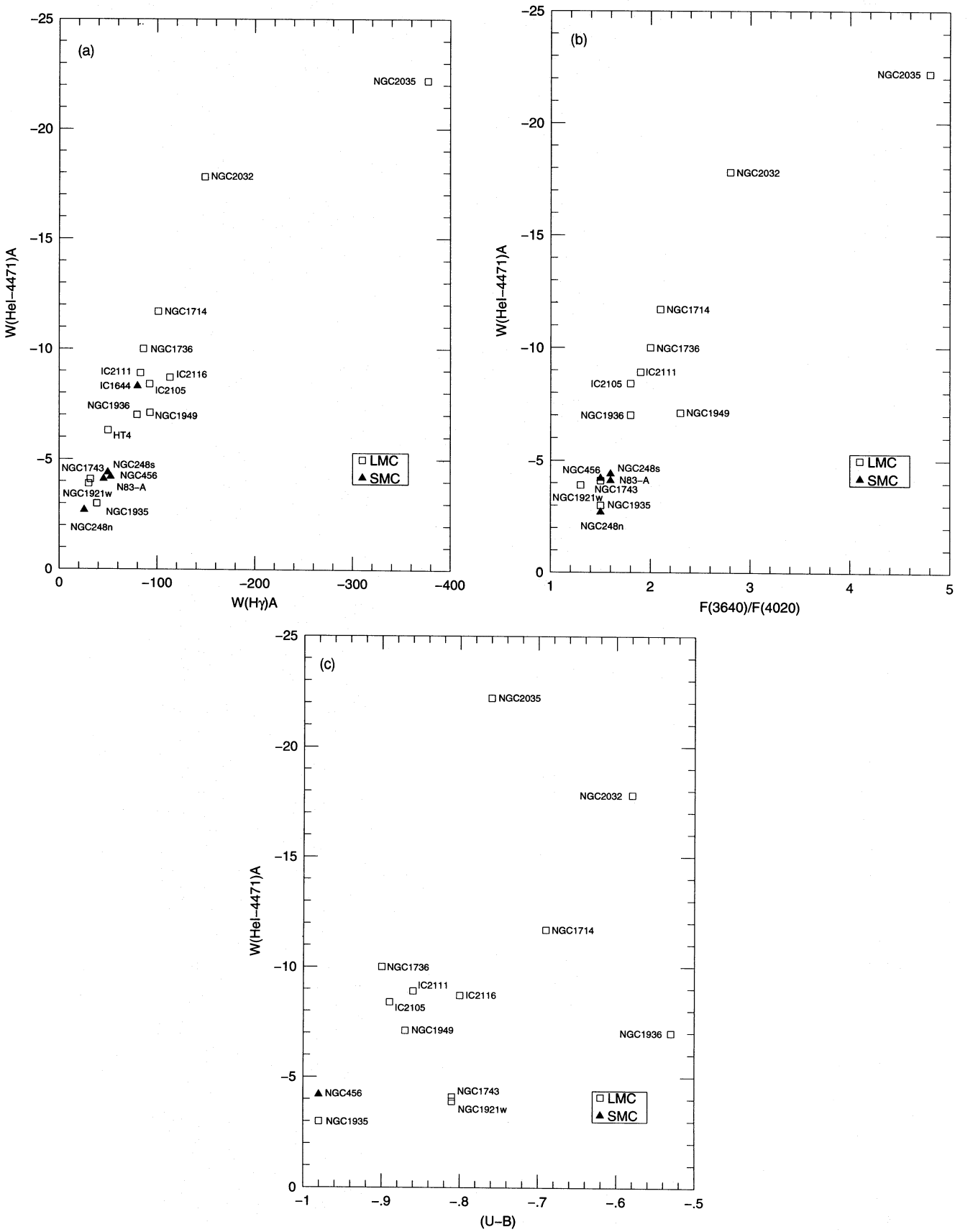

Figure 2. (a) For the H II regions the equivalent width of He I 4471 Å is plotted against that of Balmer Hγ. Symbols distinguish LMC and SMC H II regions. The equivalent width unit is angstroms. Errors are discussed in Section 3. (b) Equivalent width of He I 4471 Å against the Balmer discontinuity as measured by the flux ratio between 3640 and 4020 Å for H II regions. Symbols and units as in Fig. 2(a). (c) Equivalent width of He I 4471 Å against the integrated $(U-B)$ colour for H II regions. Symbols and units as in Fig. 2(a).

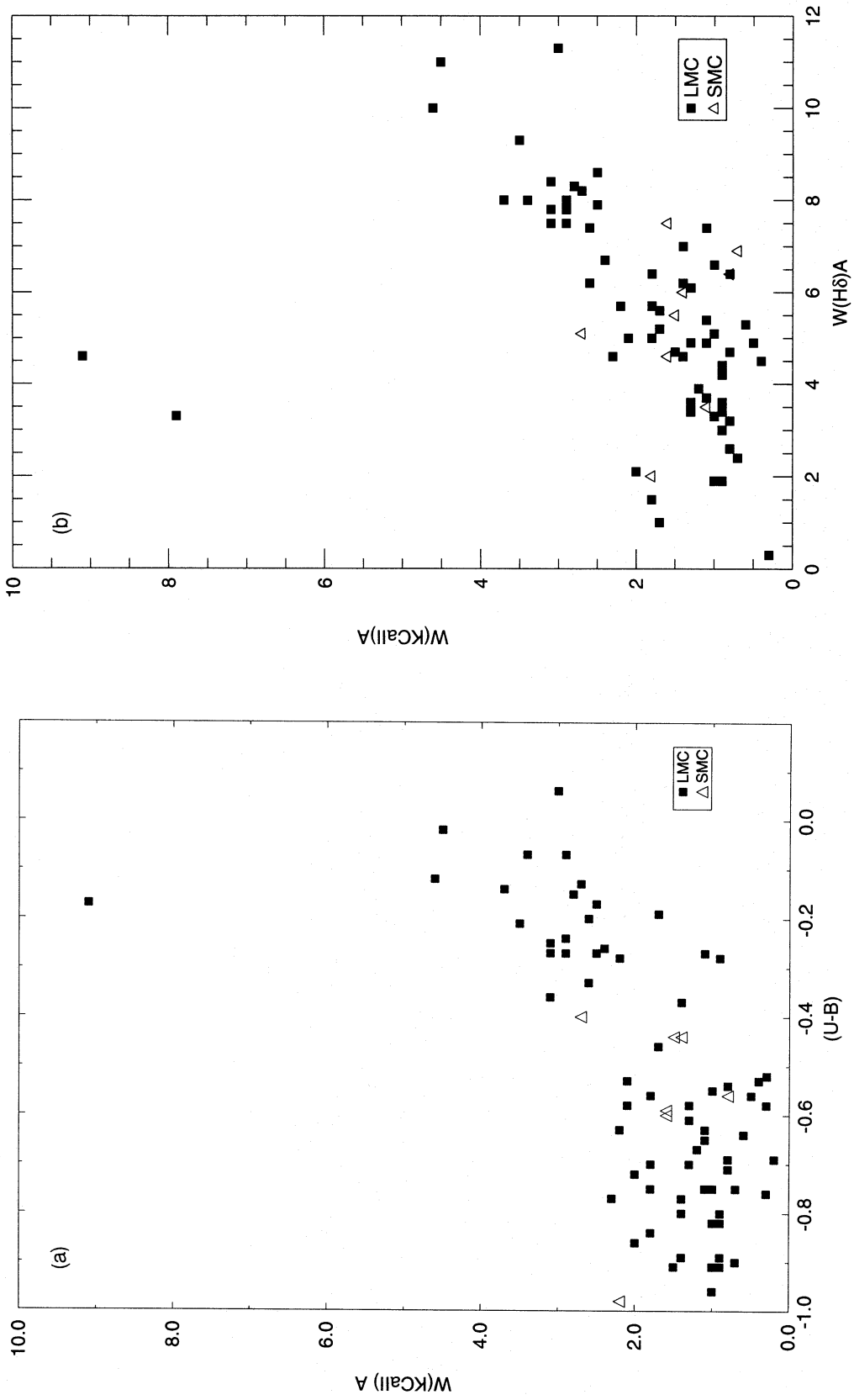

Figure 3. (a) For absorption-dominated spectra we plot the equivalent width of K Ca II against the integrated $(U-B)$ colour. Symbols distinguish LMC and SMC star clusters. Units as in Fig. 2. (b) The equivalent width of K Ca II against that of Balmer Hδ for star clusters. Symbols and units as in Fig. 3(a). (c) Equivalent width of Balmer Hγ versus Hδ for star clusters. Symbols and units as in Fig. 3(a).

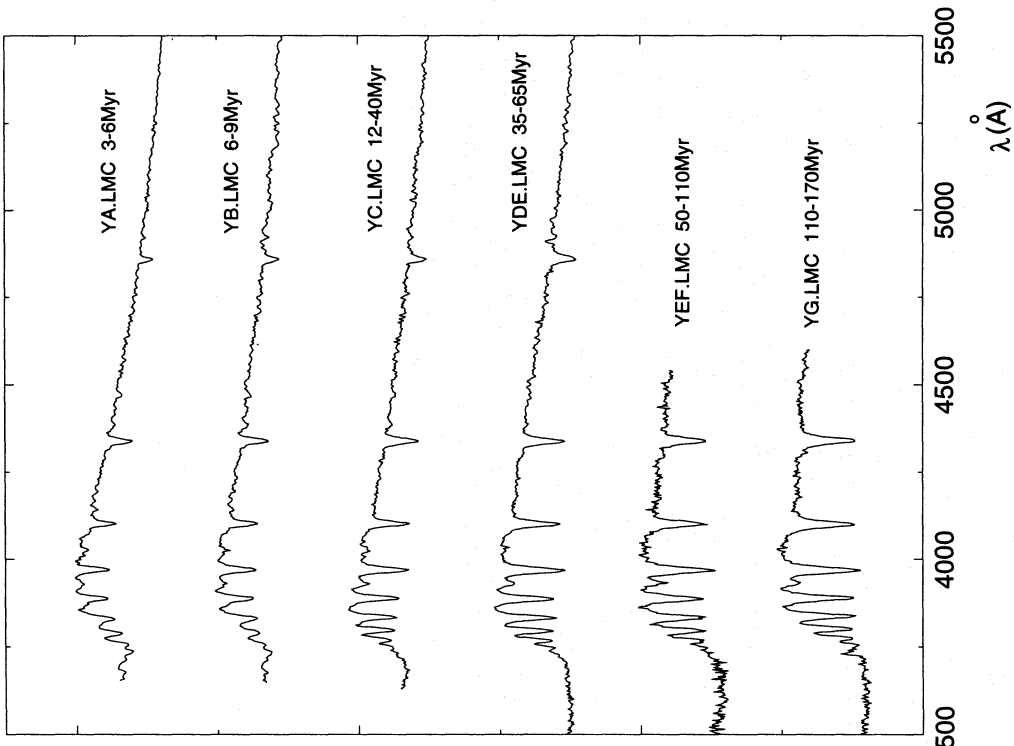

Figure 4. LMC star cluster spectral groups which are flux-dominated by turn off stars. The spectra are in F_λ units normalized to 1.0 at 4020 Å, and shifted with an additive constant when necessary.

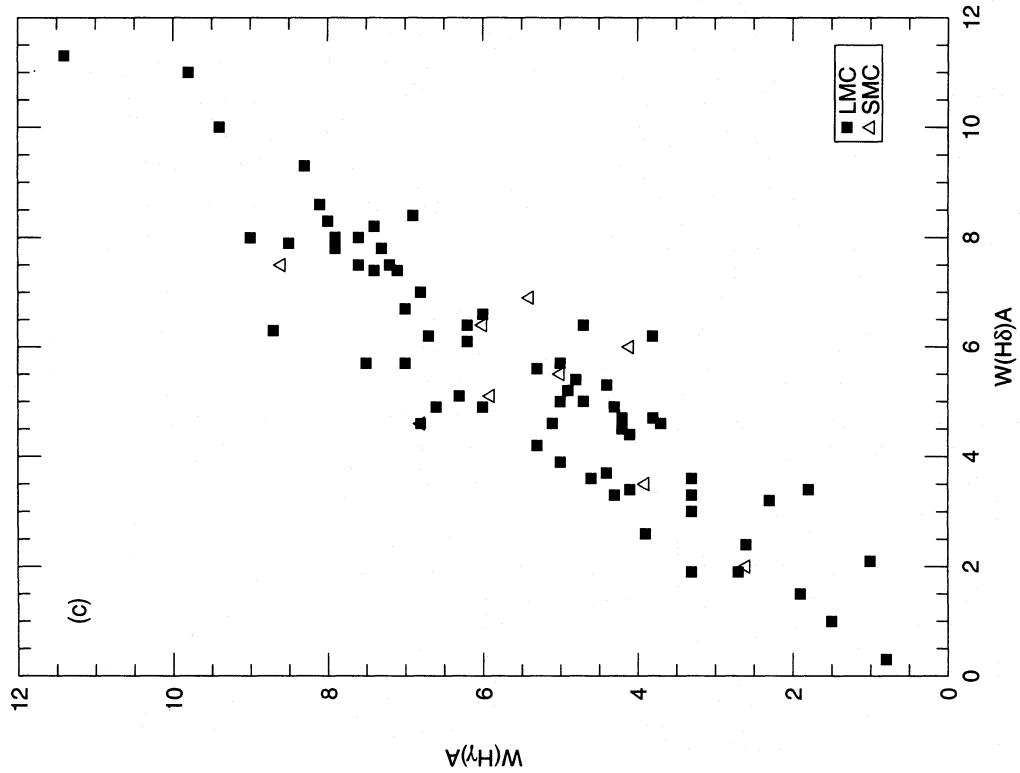

Figure 3 – *continued*

radiation; (ii) systems where stellar emission lines originating from Be, LBV or WR phases are present; and (iii) systems showing spectra with absorption features only.

In order to create templates which should represent evolutionary stages of single-burst stellar populations, in view of spectral syntheses of composite systems like galaxies, we have used the loci of the objects in diagrams such as Figs 1, 2 and 3 for grouping the cluster spectra with similar properties. Nevertheless, the ultimate decision of whether or not to average the spectra was based on the overall spectral resemblance. Thus, the criteria ordered by importance were as follows.

(1) Overall spectral resemblance, in particular continuum distribution and H Balmer line strengths.
(2) SWB type and *UBV* colour proximity.
(3) A series of diagrams involving *W*s of absorption and emission lines, as well as continuum ratios, from Tables 3, 4 and 5, mainly including He I for H II regions, and Hδ, Hγ and K Ca II for absorption-dominated spectra.

The summation of the similar spectra was weighted according to their squared S/N value from Table 1. The group members are listed in Table 6, together with age estimates based on the subsequent discussions. The group names follow those in the near-infrared spectral analysis of Magellanic Cloud clusters (BAS90); nevertheless, the larger sample and variety of spectral characteristics in the present study led us to create more groups: we obtained 24 spectral types in the LMC (including the spectrum of 30 Dor from BAS94) and 7 in the SMC.

6.1 LMC Clusters with Absorption Line Spectra

We show in Fig. 4 the LMC groups with absorption line spectra which do not show evidence of flux dominance by a few luminous evolved stars. Their overall appearance, in particular Balmer absorption and discontinuity, resemble those of the main-sequence star spectra from B0V to A0V in the spectral library of JHC84. This suggests that in the clusters, the upper main sequence with turnoff at such spectral types dominate the integrated spectrum in the blue–violet range. The template ages in Table 6 for absorption-dominated spectra are based on the ages of individual clusters in column (10) of Table 1. This age sequence can be used to compare the LMC spectral groups with the Galactic open cluster CMD properties (Mermilliod 1981a, b): e.g., YA.LMC basically corresponds to the NGC 2362 group and YG.LMC to that of NGC 2287.

The absorption-line templates showing evidence of flux dominance by supergiants of different temperatures are presented in Figs 5(a), (b) and (c). We show in each case a simple spectral synthesis combining a suitable cluster template dominated by the upper main sequence (Fig. 4) with a supergiant star from the JHC84's library with adequate temperature, in order to reproduce the overall spectral appearance. In Fig. 5(b) the metallic lines appear somewhat stronger in the model than in the cluster spectral group, owing to the fact that JHC84's supergiants (Galactic disc) present higher metallicities than those of the LMC clusters. The components are shown to scale, according to their proportion at 4020 Å.

In Fig. 5(a) we show the template YB.LMC (6–9 Myr) which presents evidence of late-type star absorption features and a flatter continuum than that of its age neighbour YA.LMC (3–6 Myr). The simple synthesis indicates that a combination of the latter template with an M2I star from JHC84 reproduces well the spectrum of YB.LMC. This red supergiant phase is well-documented spectroscopically in the near-infrared (BAS90), and is expected from stellar evolution models (GB93).

The template YC_SG.LMC consists of the clusters NGC 2096 and BRHT 16b, resembling the spectrum of intermediate temperature stars. We checked the redshift of the cluster spectra and concluded that the stars do not belong to the Galactic foreground. The simple spectral synthesis suggests F6 supergiant dominance (Fig. 5b). The age 49 Myr for NGC 2096 implied by its $(U-B)$ colour in Table 1 appears to be excessively large, which can be explained by the flux dominance of the intermediate temperature supergiant(s) affecting considerably the U and B filter bandpasses. Mermilliod's group where some F supergiants occur is that of NGC 457 at a turnoff $B1/B2$ (age $\approx$10–20 Myr). BRHT 16b is located in the association NGC 2042, where SL 601 (in YA.LMC) is also embedded. We thus conclude that the most probable age for the template cannot be more than 20 Myr, and we have adopted as the underlying population the YC.LMC template in the synthesis. Also the loci of the YC.LMC and YC_SG.LMC templates in the *UBV* integrated colour–colour plane are quite close. We conclude that NGC 2096 and BRHT 16b are cases of stochastic fluctuation on YC.LMC, where the occurrence of one (or more) luminous evolved star(s) in sparsely populated clusters has severely influenced the integrated spectra.

Fig. 5(c) shows a template (YA_SG.LMC) where hot supergiants seem to dominate the cluster integrated light. An O8 supergiant (from JHC84) reddened by $E(B-V)=0.5$ and combined to an underlying population like that of YA.LMC reproduces its spectral characteristics, in particular the Balmer discontinuity.

6.2 LMC clusters with emission line stars

Mass loss from massive stars, and its consequences (such as circumstellar emission and stellar winds which sweep the interstellar matter in the surrounding regions), has conspicuous effects on the integrated spectra. In our sample some cluster spectra show signatures of the presence of mass loss.

We show in Fig. 6 cases of cluster spectra with features of Nitrogen (WN) and Carbon (WC) Wolf–Rayet stars, as well as Be stars. The integrated spectra of LT-α and HDE 269828 (LT-β) contain WN features; LT-α also has a flat continuum and features denoting a red supergiant; the presence of these individual stars was reported by Lortet & Testor (1984). These clusters are located in the H II region/OB association complex NGC 2044 (N 157C), for which Dottori & Bica (1981, hereafter DB81) obtained an integrated $W(\mathrm{H}\beta)=-76$ Å, typical of the latest stages of H II region evolution (CPD86). The presence of a red supergiant flux contribution in LT-α also suggests some age spread in the complex.

HD 32228 is a compact cluster which contains a WC5 star [Heydari-Malayeri & Testor (1983), and references therein]. The WC feature C III–IV (4650 Å) is prominent in the integrated spectrum (Fig. 6). The cluster is located in the large

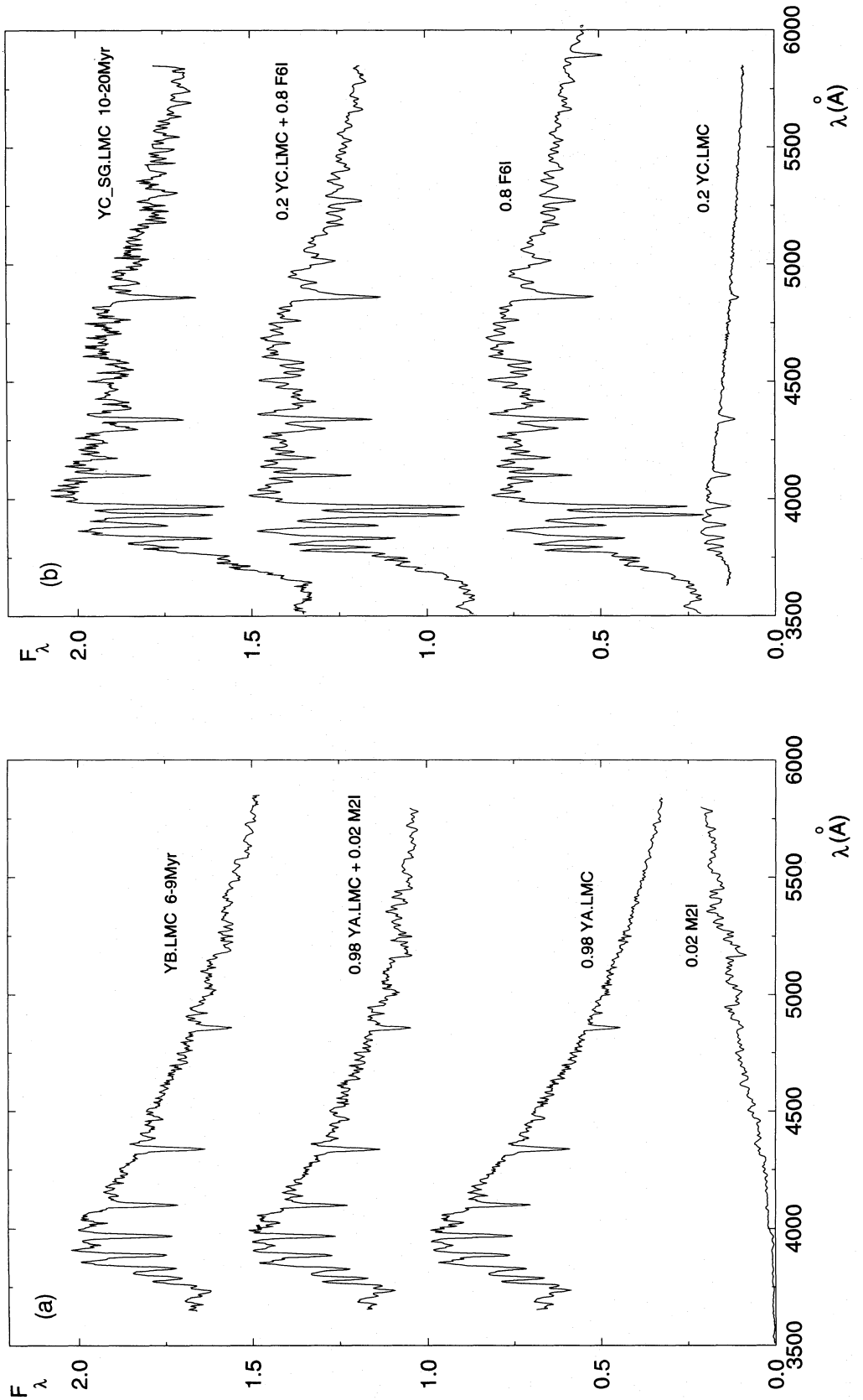

Figure 5. (a) LMC spectral group with important flux contributions from cool supergiants (SGs). We also show a simple spectral synthesis with the relative flux contributions (at 4020 Å) of a suitable turn off dominated template from Fig. 4 and a Galactic supergiant from Jacoby, Hunter & Christian's (1984) stellar library. The spectral group and the model are shifted by additive constants for clarity, when necessary. (b) Same as in Fig. 5(a), but for intermediate temperature SGs. (c) Same as in Fig. 5(a), but for hot SGs.

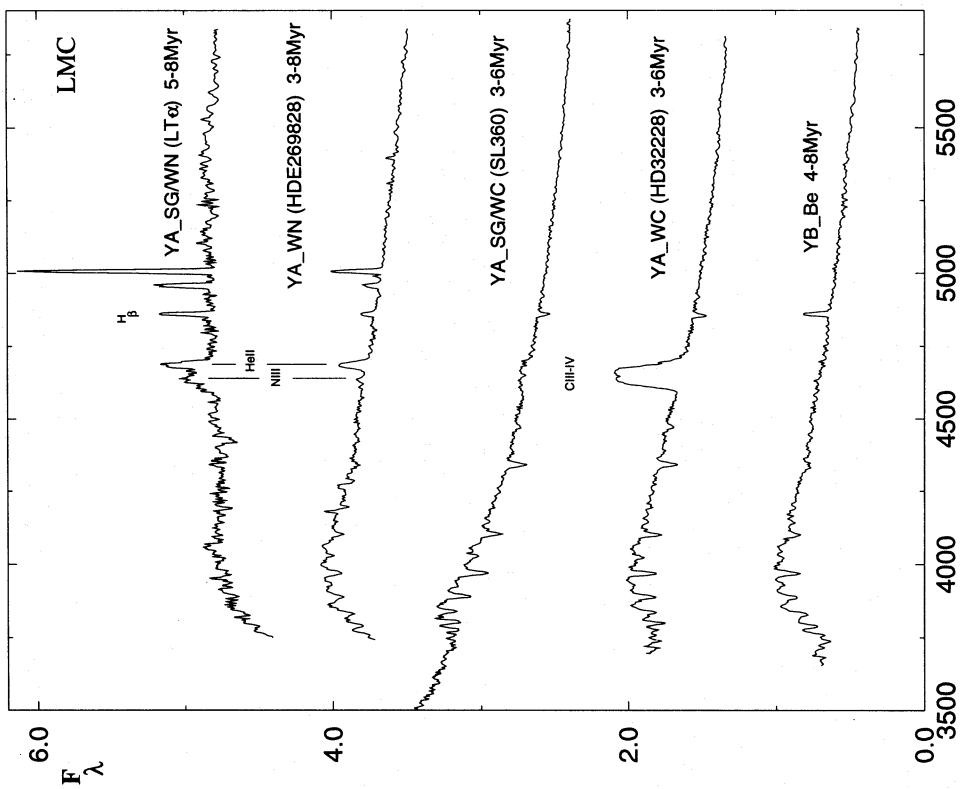

Figure 6. LMC star cluster spectra with features from emission line stars: LT-α has Nitrogen WR together with red supergiant features; HDE 269828 has Nitrogen WR; SL 360 has Carbon WR; NGC 1994 and NGC 1983 (YB-Be.LMC) have Be emission stars and cool supergiants as well.

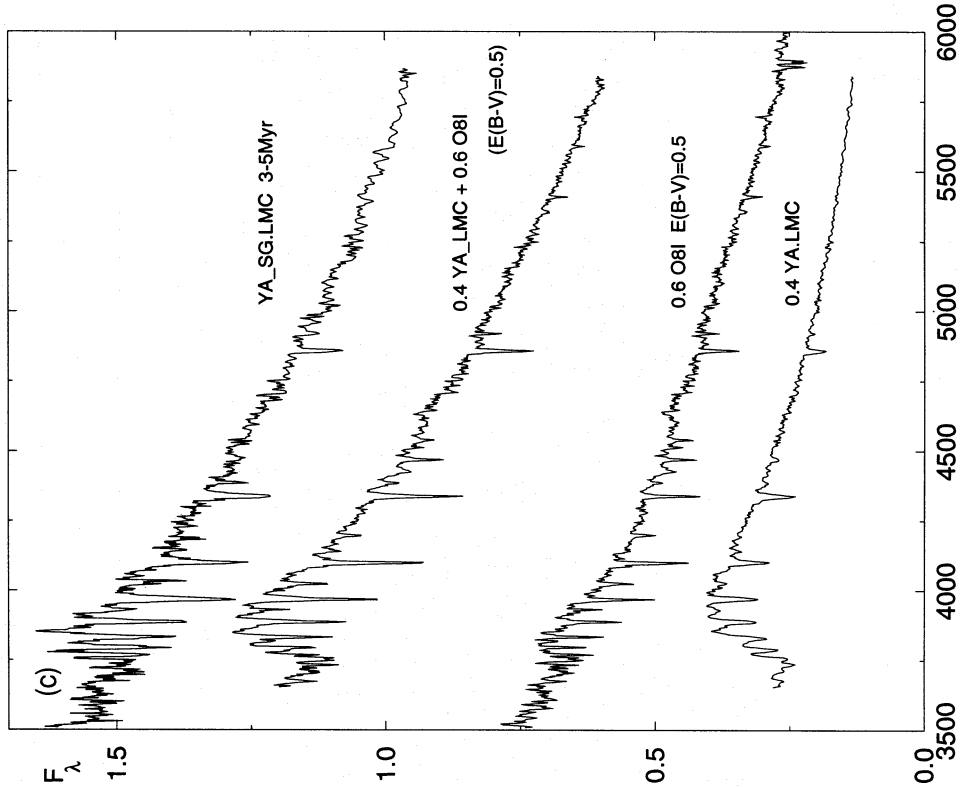

Figure 5 – *continued*

association NGC 1761 (LH9), a gas-poor region of the H II complex N 11. HD 32228 and its environment resemble the case of the Galactic cluster NGC 6231, according to Walborn & Parker (1992). These authors give an age of 5 Myr for HD 32228. As a comparison, NGC 6231 has an age of 4.5 Myr, comparable to the last evolutionary stages of H II regions, and also presents an integrated spectrum with a strong WC emission (Santos & Bica 1993). We find evidence of the WC emission feature in the LMC cluster SL 360 (Fig. 6). The emission is much weaker than that of HD 32228, certainly because of a dilution effect, since SL 360 is much more populous than HD 32228 and/or the WC star in SL 360 belongs to a later type. DB81 obtained $W(\mathrm{H}\beta) = -68$ Å and $W(\mathrm{H}\beta) = -81$ Å for the H II/OB complexes where SL 360 and HD 32228 are respectively embedded, again values corresponding to evolved H II regions.

The template YB_Be.LMC is composed of NGC 1994 and 1983, which show Hβ in emission but offer no trace of forbidden lines. This is explained in terms of Be stars, as discussed in BAS90, where NGC 1994 showed a strong Hα emission. The template also shows spectral characteristics indicating the presence of red supergiants.

The cluster H88 − 267 contains the LBV star S Doradus (Fig. 7). We made spectral extractions in our frames of the whole cluster, of the western (essentially S Dor) and of the eastern halves. The object was observed in both runs and we show the averages of the extractions. S Dor dominates the cluster spectrum, contributing ≈ 85 per cent at 4020 Å of the cluster integrated light. The age attributed for the cluster in Table 6 takes into account the ages obtained from the $(U-B)$ integrated colour, the spectral characteristics of the eastern extraction which resembles the YA.LMC template, and DB81's $W(\mathrm{H}\beta)$ value for the H II/OB complex where it is located (N 119, which also contains NGC 1910 and SL 360).

The short-lived LBV stage occurs immediately before the WN phase, its variability being associated with the slowly expanding envelope; S Dor is losing mass at a rate of 10^{-6} $M_\odot$ yr^{-1} during minimum and 10^{-4} $M_\odot$ yr^{-1} during the maximum V luminosity (Leitherer et al. 1985). It was observed to change 1.2 mag in V between 1984 November/December (minimum) and 1988 September/October (maximum) (Spoon et al. 1994). Thackeray (1974) carried out spectroscopic observations and showed that strong [Fe II] lines (4244, 4287 and 4359 Å) occur at the minimum magnitude whereas Balmer emission lines with P-Cygni profiles are dominant features at the maximum. According to the Spoon et al. (1994) light curve, S Dor had $V \approx 9.7$ and was decreasing in brightness during our run A (1991 October 31). Unfortunately their light curve ends in 1992, and the brightness is not available for our run B (1993 January 15). The features in our two spectra are similar, which suggests that in run B the star should have a V brightness comparable to that during run A.

6.3 LMC objects with strong nebular emission

The H II regions were separated into a higher [W(He I–4471 Å) < −6.5 Å] and a lower [W(He I–4471 Å) > −6.5 Å] excitation group. The resulting mean spectra are shown in Fig. 8. Notice the strong Balmer discontinuity in emission at $\lambda \approx 3646$ Å for the more excited group, as well as stronger emission lines relative to the continuum intensity, in particular those corresponding to [O III], [Ne III] and He I (see also the discussions in Section 5).

The ages of the H II region templates (Table 6) were estimated from $W(\mathrm{H}\beta)$ and the intensity ratio [O III](4959, 5007)/Hβ (the continuum is essentially the same under the three lines), with the CPD86 models at the metallicities appropriate for the LMC ($Z = 0.008$) and the SMC ($Z = 0.003$). We also used ages from Copetti, Pastoriza & Dottori (1985, hereafter CPD85) for individual H II regions. The less excited template (H IIo.LMC) is on the average older than the more excited one (H IIy.LMC).

We also show in Fig. 8 a spectrum representing the integrated light of 30 Doradus from BAS94. It is as excited as H IIy.LMC, including prominent Balmer discontinuity in emission and the He I 4471-Å line. In addition, WN features arising from the well-documented WR stars in the object (e.g. Melnick 1992) are clear. The age values in Table 6 take into account Melnick's (1985) CMD analysis and age determinations from CPD85.

The compact nebula N 63A is located in the H II region/OB association NGC 2030, and the CMD of the stellar aggregate indicates an age of 4 Myr (Laval, Greve & van Genderen 1986). The age 3–5 Myr in Table 6 also takes into account that derived by CPD85 for the H II region complex where N 63A is embedded. As shown in Laval, Greve & van Genderen (1986) and references therein, the eastern side of N 63A is the supernova remnant SNR 0535 − 66.0, whereas the western one is an H II region. We compare in Fig. 9 our spectrum of N 63A with that of the SNR N 49 taken in the same run. Low ionization emission lines such as [Fe II] and [S II] are not apparent, which indicates that the emission in our spectrum of N 63A arises mostly in the H II region component. The spatial region sampled by our spectrum also includes the central parts of the stellar aggregate. Indeed, a stellar continuum is clear in the spectrum of N 63A, as compared to that of the supernova remnant N 49.

6.4 LMC objects with weak nebular lines

In addition to the H II regions, the sample contains absorption-line spectrum clusters with weak nebular lines superimposed.

We show in Fig. 10(a) the spectrum of HDE 268726 (E1.LMC), a possible transition case between H II regions and more evolved systems, by the presence of a low-excitation emission spectrum. It is located at the edge of the large H II region/OB association NGC 1763 (N 11B). The central object has been classified as a B2II star (Parker et al. 1992). Heydari-Malayeri & Testor (1983) found an 8 arcsec emission blob surrounding the central object. In Fig. 10(a) the continuum distribution of its integrated spectrum resembles that of a B2V star from JHC84, which has been reddened by $E(B-V) = 0.20$, or conversely that of the YA.LMC template. We emphasize that an integrated spectrum is a brightness-weighted average over the individual stellar spectra of a cluster; then, although these spectra resemble that of a B2V star, the clusters involved should contain earlier spectral types, consequently still providing ionizing photons to the environment. In fact, the NGC 2362 group in Mermilliod (1981a,b), with turnoff in B0, is of a similar age to that of YA.LMC. The Balmer emission lines in the observed range

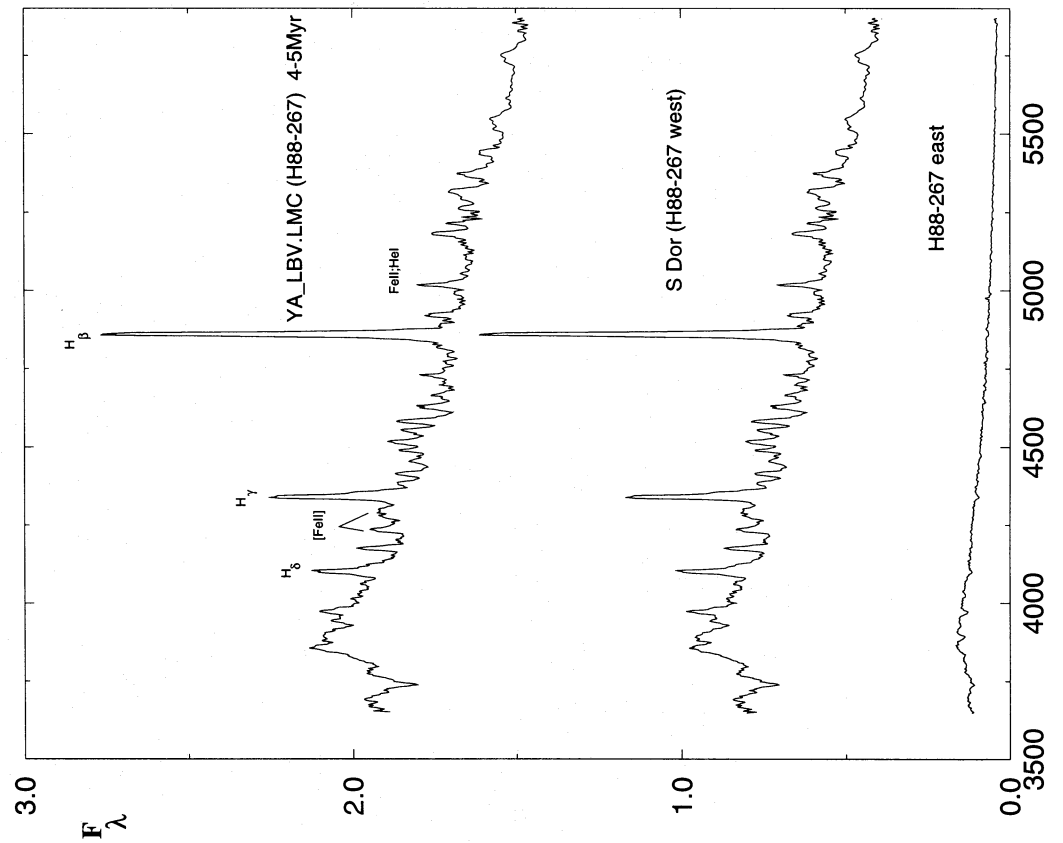

Figure 7. Spectrum of the cluster H88-267. The western part is dominated by the Luminous Blue Variable S Doradus, which is shown as the scale flux with the eastern part, which resembles the turn off dominated template YA_LMC (Fig. 4).

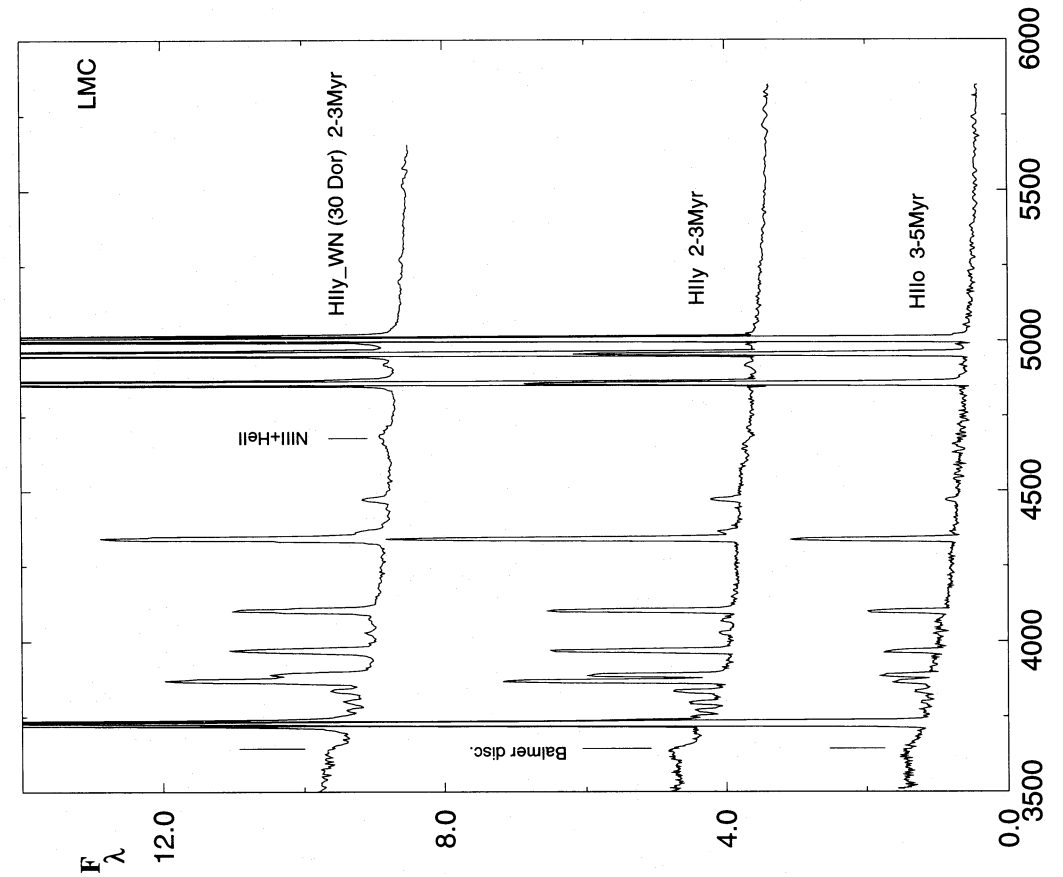

Figure 8. Spectral groups of LMC H II regions. In addition to the more excited (younger) and less excited groups, we show the spectrum from BAS94 representative of the integrated properties of 30 Doradus, which has a contribution from Nitrogen WR stars.

Table 6. Spectral groups.

Group	Members NGC	Age Range (Myr)
H IIy.LMC	IC 2105 1714 IC 2111 1736 IC 2116 1936 1949 2032 2035	2–3
H IIo.LMC	1743 HT 4 1921w 1935 SBCPGD1	3–5
H IIy_WN.LMC	2070 (30 Dor)	2–3
HII+CL+SNR.LMC	N 63A	3–5
YA.LMC	Rob 1 1967 HS 314 1984 SL 538 KMHK 1074 SL 586 2102	3–6
YA_SG.LMC	1731 SL 82 1970 SL 492 SL 601 2011	3–5
YA_WC.LMC	HD 32228	3–6
YA_SG/WC.LMC	SL 360	3–6
YA_LBV.LMC	H88-267	4–5
YA_WN.LMC	HDE 269828	3–6
YAB_SG/WN.LMC	LT–α	5–8
YB.LMC	KMHK 212 1767 1805 2002 2006 HS 385 2009 BRHT 14b M-OB4 2091 2098 2100	6–9
YBA_Be.LMC	1983 1994	4–8
YC.LMC	1711 1735 1772 1782 1818 1847 1951	12–40
YC_SG.LMC	BRHT 16b 2096	10–20
YDE.LMC	1755 1774 SL 153 1850 1903 2025 2136 2159 2164 2214	35–65
YEF.LMC	2041 2058 2134 2156	50–110
YG.LMC	1872	110–170
E1.LMC	HDE 268726	4.5–6.5
E2.LMC	2021 BCDSP 8	3–5
E3.LMC	LT–ζ LT–γ LT–δ	4–8
E4.LMC	SL 639 2092	6–12
E5.LMC	2147	6–20
E6.LMC	1921e 1854	20–40
H IIy.SMC	IC 1644	2.5–3
H IIo.SMC	248n 248s 456 N83A	3–3.5
YA.SMC	K 50	5–8
YA_SG.SMC	Sk 157 Sk 158	3–5
YB.SMC	299	8–12
YB+.SMC	K 54	6–10
YC.SMC	L 56 330 376 796	10–20

appear to be drowned in the absorptions, only Hβ and Hγ definitely being in emission. The central object might be interpreted as a small compact cluster containing a hot supergiant. The clusters in the YA.LMC group, with comparable spectral distribution, present an absorption-line spectrum only, which suggests that their interstellar medium has been swept by stellar winds. A possible explanation for the presence of gas in HDE 268726 might be that the blob is physically contained by the gas of the larger complex, postponing the expansion.

Fig. 10(b) shows the remaining cases. E2.LMC consists of NGC 2021 and BCDSP 8, both of type SWB 0, and within large H II/OB complexes (Table 1). E3.LMC is formed by LT–γ, LT–δ and LT–ζ, which are embedded in the H II/OB complex NGC 2044 together with two clusters including WR stars (Section 6.2). The forbidden lines in the spectrum of the clusters might be explained by local gas filaments or blobs. E4.LMC consists of SL 639 and NGC 2092, which are SWB I clusters having a flat continuum, probably caused by red supergiants. SL 639 is at the edge of the N 157 complex (which includes 30 Doradus) and apparently has an associated emission region (see the ESO/SERC Sky Survey, plate R, field 57). NGC 2092 lies within the association LH111, which also includes the populous blue cluster NGC 2100; the association shows some emission filaments and it is embedded in the much larger emission complex DEM 310. One such filament is superimposed on NGC 2092 (see the ESO/SERC Sky Survey, plate R, field 57). We conclude that SL 639 and NGC 2092 are probably members of the star-forming complexes, but belong to their older parts. E5.LMC is the cluster NGC 2147 (SWB I), lying near the edge of the H II region N 75B. The cluster absorption lines and Balmer discontinuity marginally suggest a connection to the star-forming complex in terms of age. E6.LMC contains NGC 1921e and 1854. The latter object is a populous cluster of type SWB II. It is apparently superimposed on the edge of N 105 (=DEM 86), which contains in its central parts the H II region/OB association NGC 1858. A sharp edge of the H II region crosses NGC 1854; the cluster CMD in Alcaino & Liller (1987) indicates an age of 25 ± 6 Myr from the turnoff at $V \approx 14.5$. This cluster is clearly too old to be the ionizing source of the emission. NGC 1921e (SWB II) seems to be a similar case. It is embedded in the H II region DEM 133 and is located on its sharp edge. NGC 1921e constitutes a pair with NGC 1921w (=N 121), which is a compact H II region (Table 1). The absorption lines and Balmer discontinuity of NGC 1854 and 1921e suggest an age > 20 Myr. Such cases of non-coeval superposition could be simple projections, or it may be that the star cluster might happen to be embedded in a current star-forming environment. Another possible explanation for some of these composite spectra is that one is detecting gas emission from SNRs that appears as a result of the evolution of the cluster massive stars.

The oldest cluster in the sample NGC 1872 (YG.LMC) is also superimposed on an emission region (N 113). However, the emission is uniform around the cluster and the background subtraction in the CCD frame cancelled out the emission lines in the cluster spectrum (Fig. 4).

6.5 Evolution shown on the $(U-B) \times (B-V)$ diagram

Using the integrated *UBV* data from Table 1 we calculated the mean locus of each LMC spectral group (Table 6) on the $(U-B) \times (B-V)$ plane and plotted them in Fig. 11. Considering the ages in Table 6, the continuous line in Fig. 11 is the normal evolutionary path for the objects whose spectral characteristics do not depend on the presence of very few luminous evolved stars. The group H IIy.LMC, consisting of more excited (younger) H II regions, has redder $(U-B)$ colour than that of its less excited (older) counterpart H IIo.LMC. Consequently, the youngest H II regions do not occupy the upper left corner of the integrated colour–colour diagram and the evolutionary path is bent into a hook shape at that point. At first glance, this effect might be thought to be caused by more dust in the younger group. In order to check this, we have eliminated the emission lines from the spectra of the H IIy.LMC and H IIo.LMC groups and convoluted them with the *U* and *B* filters. The H IIy.LMC continuum colour was 0.29 mag bluer in $U-B$ and 0.08 bluer in $B-V$, which rules out the dust absorption hypothesis. The effect is caused by the distribution and relative intensities of emission lines in the filter bandpasses. Indeed, the *U* filter ($\lambda_0 \approx 3600$ Å, FWHM ≈ 800 Å) includes [O II] (3727 Å) and the *B* filter ($\lambda_0 \approx 4400$ Å, FWHM ≈ 1000 Å) includes the

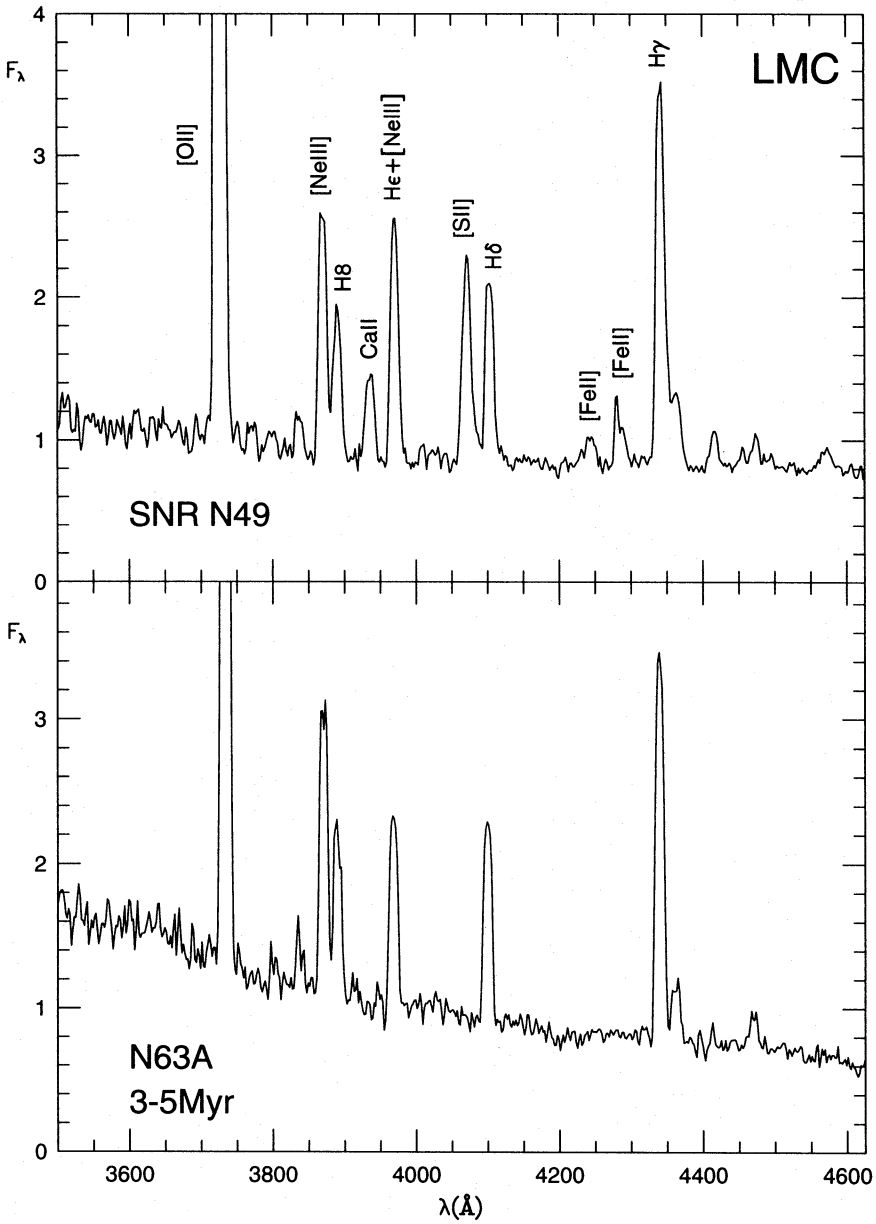

Figure 9. Spectrum of the LMC compact nebula N 63A is compared to that of the supernova remnant N 49 in the LMC. The spectra are normalized to the same $W(H_\gamma)$.

Balmer series from Hε to Hβ and He I (4471 Å), as well as the strong [O III] lines (4959 and 5007 Å) in its red wing. Since the flux ratios [O III]/H(Balmer) and H(Balmer)/[O II] increase for more excited H II regions, the B flux increases relative to that in U, producing redder $U-B$ colours for the more excited H II regions (Fig. 2c).

One of the absorption-dominated templates in the normal evolutionary path of Fig. 11 is YB.LMC, containing red supergiants which occupy a clump in the cluster CMDs, corresponding to the NGC 884 group of Mermilliod (1981a). This is the red supergiant phase (BAS90), which is a natural consequence of stellar evolution in populous clusters (GB93). The templates with stellar emission, as well as those with hot and intermediate temperature supergiants, contain products of fast stages of the evolution of massive stars and consequently stochastic effects determine their occurrence or not, even in populous star clusters. In Fig. 11 we connected the templates of these rare objects by means of dashed lines to approximately coeval templates in the normal ageing sequence.

6.6 SMC spectral groups

The sample of SMC objects that we observed is a factor of 6 smaller than that of the LMC, and the integrated *UBV* information is not as complete as for the LMC. Nevertheless, the spectral measurements of SMC objects in Tables 3, 4 and 5, together with comparisons with LMC templates, allow us to classify them into seven groups as shown in Table 6, all with counterparts in the LMC. The SMC templates represent

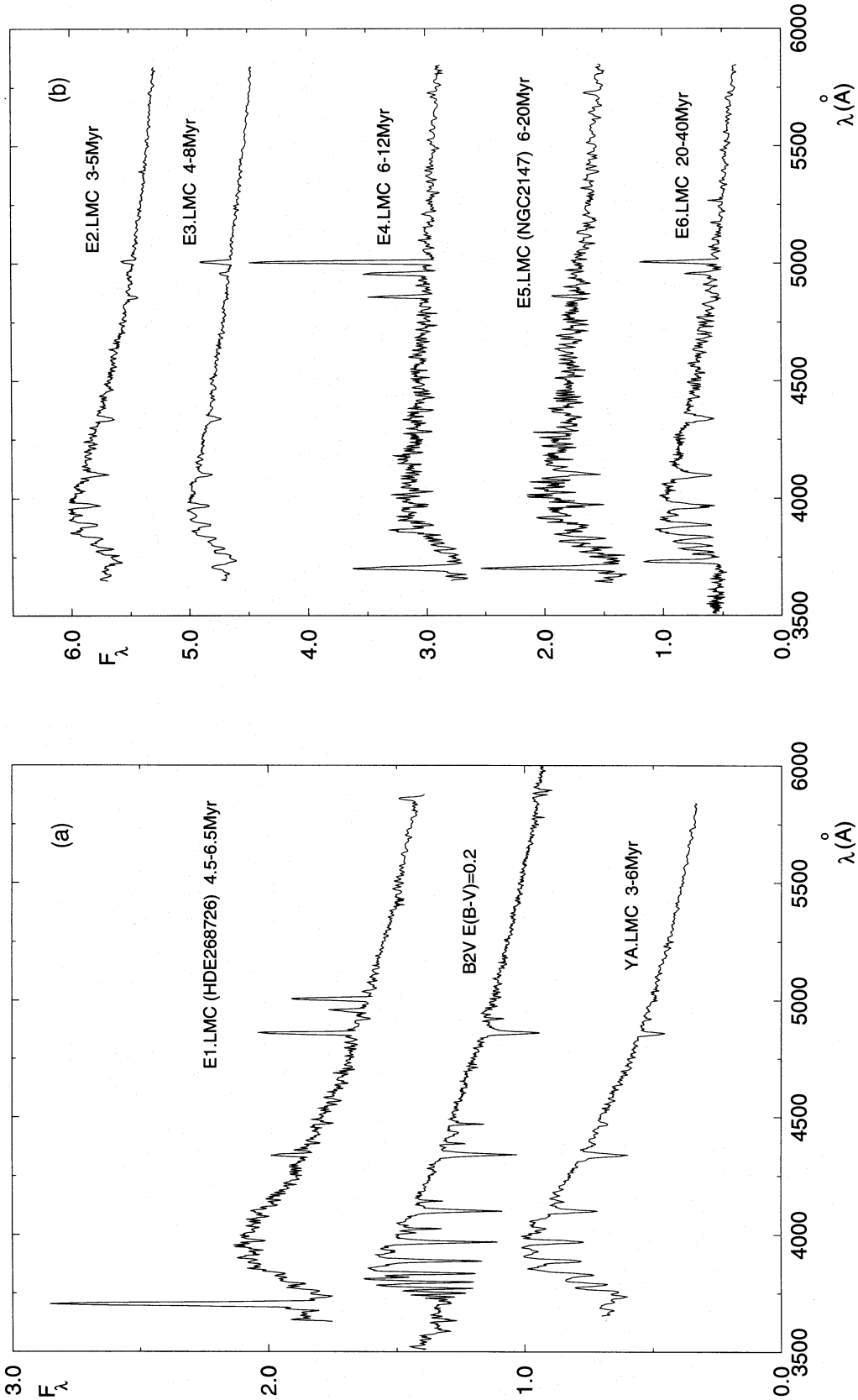

Figure 10. (a) Spectrum of the LMC object HDE 268726 with low-excitation nebular lines, compared to the YA.LMC template from Fig. 4 and to a B2 V star from Jacoby, Hunter & Christian (1984), reddened by $E(B-V) = 0.20$. (b) LMC star clusters with weak nebular lines. E2 to E4 are apparently ageing components of currently star-forming complexes; E5 may not be associated with the respective H I/OB complex, whereas E6 appears to be projected or even embedded star clusters belonging to an older generation not connected to the respective complexes.

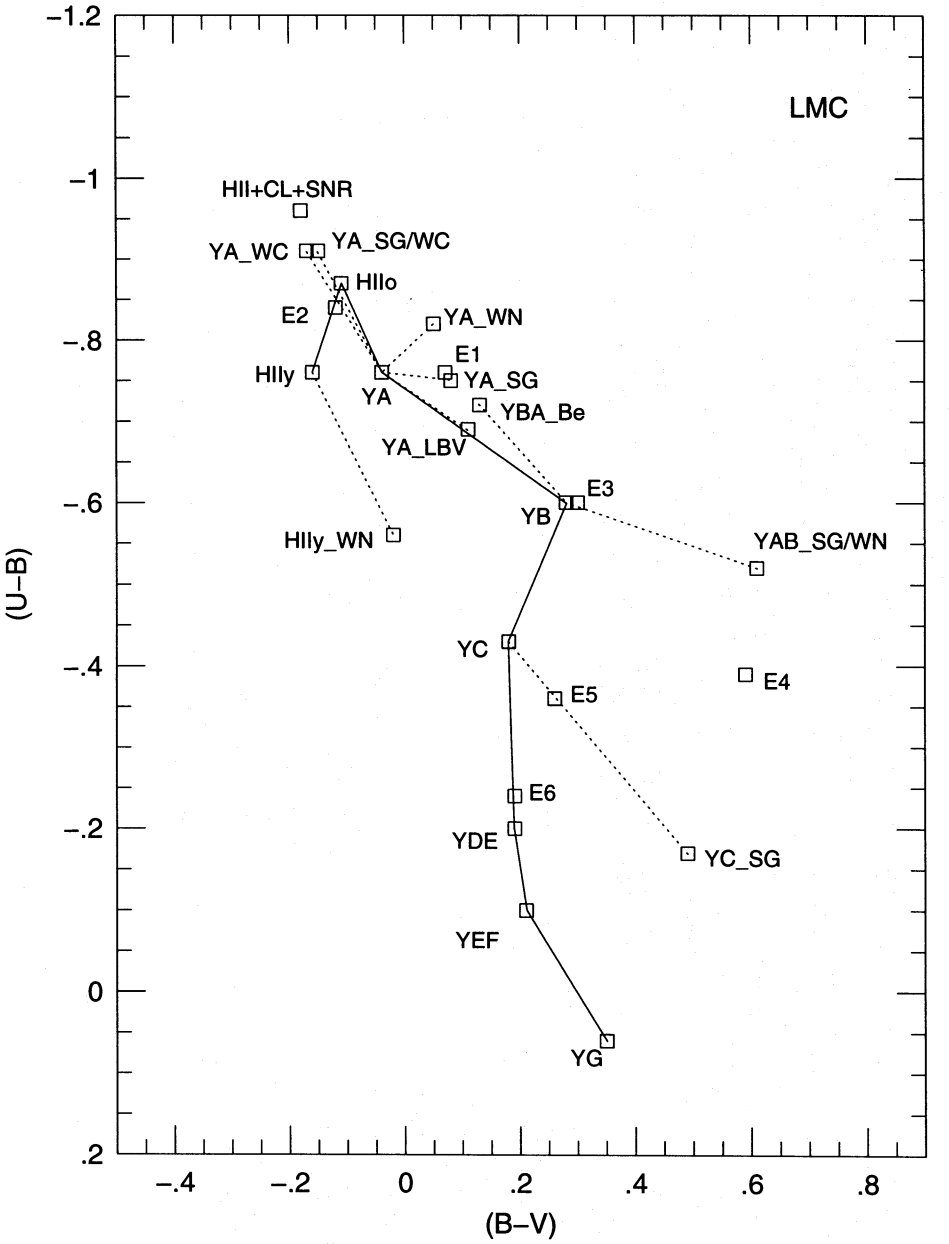

Figure 11. The distribution of the mean loci for the LMC templates on the integrated *UBV* colour–colour diagram. We connect with continuous lines the evolution of the templates for which spectral properties are not determined by only a few luminous stars. Dashed lines connect rarer objects to approximately coeval templates in the normal path.

cluster evolutionary stages for a lower metal content. Objects in the more and less excited H II region templates in the SMC, shown in Fig. 12(a), were separated with the same criteria as those in the LMC (Section 6.3).

The absorption-dominated templates are shown in Fig. 12(b). YA_SG.SMC consists of the compact clusters Sk 157 and 158 in the NGC 465 association. Hot supergiants are present in their spectra, similar to that of the YA_SG.LMC group (Fig. 5c). Indeed previous spectral classifications indicate a B0Ia type for Sk 158 and O9.5:III for Sk 157 (Lortet & Testor 1988). Alternatively, the classification of Sk 157 as a giant might come from the composite nature of the object, as a mixture of the luminosity classes I and V. The template YB.SMC (NGC 299) is flatter than YA.SMC (K 50), denoting the presence of red supergiants in the former. The near-infrared study by BAS90 clearly showed the presence of these red supergiants in NGC 299, as denoted by the enhanced Ca II triplet lines and flat continuum. In the template YB+.SMC (K 54) the red supergiant contribution is strong even in the blue, probably owing to a stochastic effect, because the cluster is much less populated than NGC 299; we checked the radial velocity of the star in our spectrum, and this indicated that it does not belong to the Galactic foreground. The YC.SMC group includes the large blue clusters NGC 330 and 376, the compact one L 56, as well as NGC 796 far away at the tip of the SMC Wing.

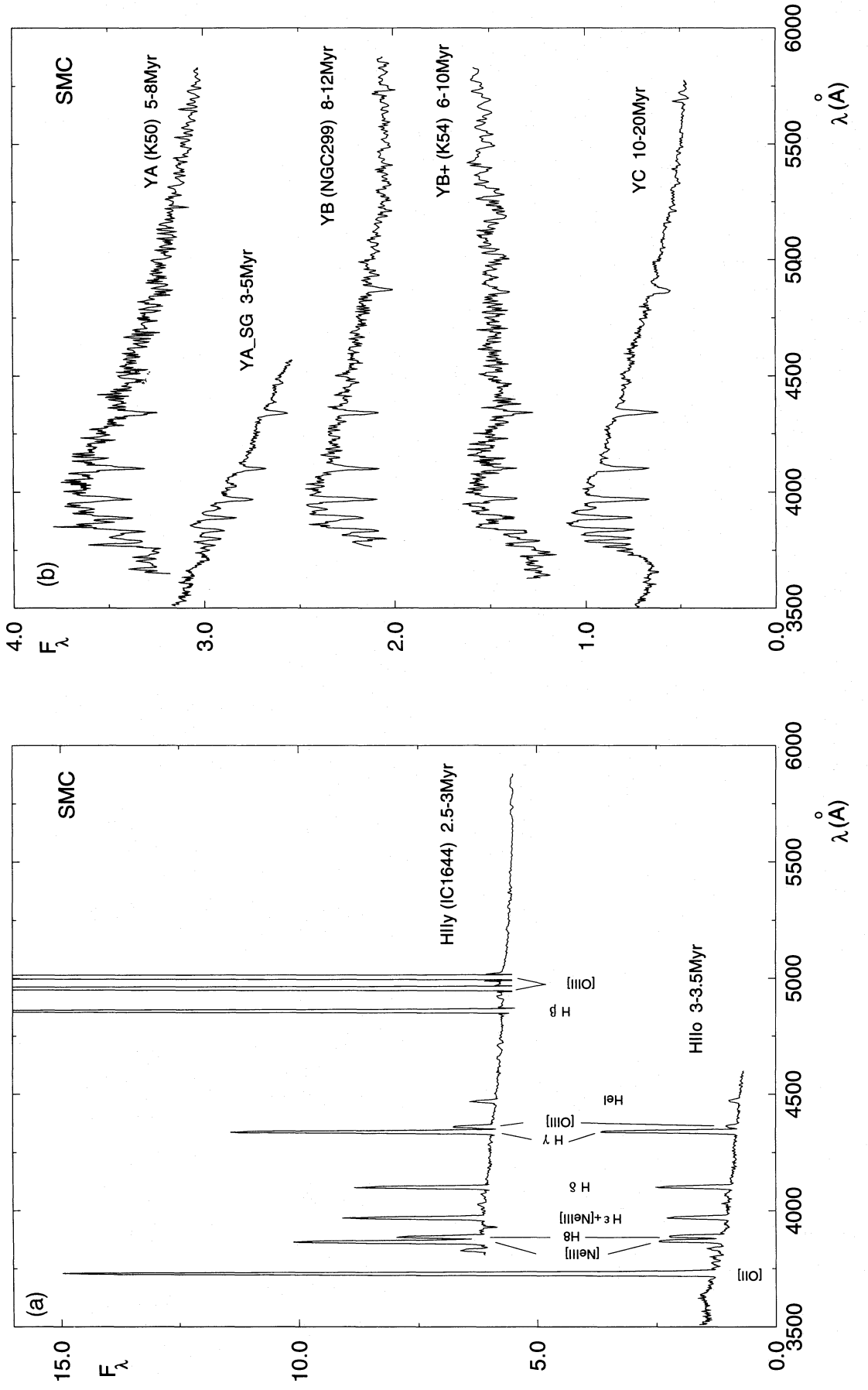

Figure 12. (a) SMC groups: H II regions. (b) SMC groups: absorption-dominated spectra.

7 CONCLUDING REMARKS AND PROSPECTIVE STUDIES

We obtained blue–violet integrated spectra of 83 young star clusters in the LMC and 14 in the SMC for evolutionary stages from as young as H II regions to as old as a few hundred Myr.

The youngest H II regions and respective stellar content, when compared to older ones, have integrated spectra with larger equivalent widths of emission lines, showing e.g. a stronger He I (4471 Å), and a prominent Balmer discontinuity in emission. The latter characteristic is explained by the combination of (i) essentially no Balmer absorption discontinuity dominating the integrated flux in O stars, with (ii) the spectral distribution of the gas emission. In the integrated $(U-B)\times(B-V)$ diagram these younger H II regions are on average ≈ 0.15 mag redder in $(U-B)$ than their less excited counterparts, which is caused by the emission line intensities and their distribution in the filters.

The sample includes integrated spectra of star clusters, with signatures of massive stars with circumstellar matter in stages such as WN, WC, LBV and Be, as well as supergiants of different temperatures. We also observed a star cluster embedded in an SNR. Several clusters show low-excitation nebular lines in their spectra; we conclude that some of them belong to ageing parts of currently star-forming complexes, whereas others are considerably older than the complexes suggesting projection or even spatial connection of non-coeval systems.

The analysis of equivalent widths and continuum distribution led us to classify the objects into various evolutionary stages. As prospective work we intend to generate spectral models by combining the template spectra for the simulation of young composite stellar populations, such as those arising from continuous star formation or bursts of different mean age and duration. The time resolution is larger and the variety of spectral types in the present template library of young clusters is richer than that used in the spectral simulations of bursts superimposed on old metal-rich (Bica, Alloin & Schmidt 1990) and old metal-poor (Schmidt, Alloin & Bica 1995) underlying stellar populations. The spectral library will be also useful for population syntheses of star-forming galaxies.

ACKNOWLEDGMENTS

We thank the CASLEO staff for their hospitality and assistance during our observations. Partial support from the Argentinian Institutions CONICET and CONICOR is gratefully acknowledged by two of us (JJC and AEP). JFCSJ acknowledges a fellowship from the Brazilian Institution FAPERGS. EB and HD acknowledge support from the Brazilian Institutions CNPq and FINEP. We also acknowledge a grant from the Vitae Foundation. We are grateful to the referee, Dr R. Terlevich, for interesting remarks.

REFERENCES

Alcaino G., Liller W., 1987, AJ, 94, 372
Bhatia R. K., Read M. A., Hatzidimitriou D., Tritton S., 1991, A&AS, 87, 335
Bica E., 1988, A&A, 195, 76
Bica E., Alloin D., 1986, A&A, 162, 21 (BA86)
Bica E., Alloin D., 1987, A&A, 186, 49 (BA87)
Bica E., Alloin D., Santos J. F. C., Jr, 1990, A&A, 235, 103 (BAS90)
Bica E., Alloin D., Schmidt A., 1990, MNRAS, 242, 241
Bica E., Alloin D., Schmitt H., 1994, A&A, 283, 805 (BAS94)
Bica E., Clariá J. J., Dottori H., 1992, AJ, 103, 1859 (BCD92)
Bica E., Clariá J. J., Dottori H., Santos J. F. C., Jr, Piatti A. E., 1995, ApJS, in press (BCDSP95)
Cid-Fernandes R., Jr, Dottori H., Gruenwald R., Viegas S., 1992, MNRAS, 255, 165
Copetti M. V. F., Pastoriza M. G., Dottori H., 1985, A&A, 152, 427 (CPD85)
Copetti M. V. F., Pastoriza M. G., Dottori H., 1986, A&A, 156, 111 (CPD86)
Dottori H., Bica E., 1981, A&A, 102, 245 (DB81)
Girardi L., Bica E., 1993, A&A, 274, 279 (GB93)
Gutiérrez-Moreno A., Moreno H., Cortés G., Wenderoth E., 1988, PASP, 100, 973
Heydari-Malayeri M., Testor G., 1983, A&A, 118, 116
Hodge P., 1961, ApJ, 133, 413
Jacoby G. H., Hunter D. A., Christian C. A., 1984, ApJS, 56, 257 (JHC84)
Kontizas M., Morgan D. H., Hatzidimitriou D., Kontizas E., 1990, A&AS, 84, 527
Laval A., Greve A., van Genderen A. M., 1986, A&A, 164, 26
Leitherer C., Appenzeller I., Klare G., Lamers H. J. G. L. M., Stahl O., Waters L. B. F. M., Wolf B., 1985, A&A, 153, 168
Lortet M. C., Testor G., 1984, A&A, 139, 330
Lortet M. C., Testor G., 1988, A&A, 194, 11
Melnick J., 1985, A&A, 153, 235
Melnick J., 1992, in Tenorio-Tagle G., Prieto M., Sánchez F., eds, III Canary Islands Winter School of Astrophysics, Star Formation in Stellar Systems. Cambridge Univ. Press, Cambridge, p. 255
Mermilliod J. C., 1981a, A&AS, 44, 467
Mermilliod J. C., 1981b, A&A, 97, 235
Mould J., Aaronson M., 1980, ApJ, 240, 464
Parker J. Wm, Garmany C. D., Massey P., Walborn N. R., 1992, AJ, 103, 1205
Rabin D., 1982, ApJ, 261, 85
Sandage A., Tammann G. A., 1981, A Revised Shapley–Ames Catalog of Bright Galaxies. Carnegie Institution of Washington Publication 635
Santos J. F. C., Jr, Bica E., 1993, MNRAS, 260, 915
Schmidt A., Alloin D., Bica E., 1995, MNRAS, 273, 945
Searle L., Wilkinson A., Bagnuolo W., 1980, ApJ, 239, 803 (SWB80)
Seaton M. J., 1979, MNRAS, 187, 73
Spoon H. W. W., de Koter A., Sterken C., Lamers H. J. G. L. M., Stahl O., 1994, A&AS, 106, 141
Stone R. P. S., Baldwin J. A., 1983, MNRAS, 204, 347
Terlevich R., Melnick J., 1985, MNRAS, 213, 841
Thackeray A. D., 1974, MNRAS, 168, 221
van den Bergh S., 1981, A&A, 46, 79
van den Bergh S., 1991, ApJ, 369, 1
Walborn N. R., Parker J. Wm, 1992, ApJ, 399, L87
Westerlund B. E., 1990, A&AR, 2, 29